# Analysis of the transient response of an automatic dynamic balancer for eccentric rotors

K. Green, A. R. Champneys, M. I. Friswell

*Bristol Laboratory for Advanced Dynamics Engineering*
*University of Bristol, Queen's Building, University Walk*
*Bristol BS8 1TR, UK*

**Abstract**

This paper investigates the transient response of a dynamical system modelling an automatic dynamic balancing mechanism for eccentric rotors. By using recently developed computational techniques, pseudospectra of the linearisation of the system about an equilibrium are computed. This approach allows one to quantify which eigenvalues are most sensitive to perturbation. It is shown how the sensitivity of the eigenvalues directly influences the transient response. Furthermore, the effect which a variation of the damping coefficients has on the pseudospectra structure is considered. A transient growth due to the non-normality of the linearised system is shown to lead to an exponential decay or to a collapse back to the stable equilibrium; these effects are identified with the changes in the sensitivities of the eigenvalues under variation of the damping parameters. This provides a new insight into the full nonlinear system, in which qualitatively similar transient responses are shown to occur.

*Key words:* Pseudospectra, non-normality, transient growth, basin of attraction

## 1 Introduction

The transient behaviour in linear dynamical systems can be very different to that predicted by a linear stability analysis, where the eigenvalues determine the asymptotic behaviour. This is a characteristic feature of linear systems with high non-normality, that is, with non-orthogonal eigenfunctions. Typically, in stable non-normal systems, transients may exhibit an undesired dynamic response, such as, a large transient growth (or apparent instability). This may be followed by a long, highly oscillatory, exponential decay or, alternatively, a rapid collapse before eventual asymptotic decay to the stable

equilibrium. Such behaviour is of particular concern when considering a linearisation about an equilibrium of a system with strong nonlinearities. In this case, a large transient growth may result in a trajectory of the full nonlinear system coming close to regions of state space where the linearisation breaks down, thus escaping the basin of attraction of the equilibrium [6,9,21]. In other words, the eigenvalues of the linearisation do not always correctly predict the behaviour of the full nonlinear system, particularly in a finite time interval [8].

In this paper, we consider the transient behaviour of an eccentric rotor fitted with an automatic dynamic balancing (ADB) mechanism [3,7,18]. This device consists of a finite number of balls which are free to move in a race at a fixed distance from the centre of rotation of the rotor, eventually balancing any eccentricity in the rotor. Possible applications of an ADB include the balancing of optical disc drives [10,11], washing machines [1], and machine tools [16]. However, principally due to unexpected instabilities, this device has never been successfully used in a commercial application. This motivates a study into the dynamics of the ADB using advanced numerical techniques.

In Ref. [7] an in-depth nonlinear bifurcation analysis, using numerical continuation [4], of the equations of motion describing the ADB was presented. This analysis identified the existence of a stable, balanced steady state equilibrium for all rotation speeds above a critical value. For certain parameters, this stable balanced state was shown to coexist with stable periodic and more complex, chaotic solutions. However, even for parameter configurations where the stable balanced state is easily achieved, direct numerical integration of the governing equations of motion showed a long, high amplitude, oscillatory transient before stability was reached. In many applications such transient effects would be highly undesirable. This transient behaviour motivates further investigation into the sensitivity of the stable balanced state of the ADB.

After linearising the equations of motion around a steady state, sensitivity of the eigenvalues to perturbation can be measured in a number of ways. The concept of pseudospectra [5,20] is a recently developed tool which allows one to quantify which eigenvalues of the linearised system are most sensitive to perturbation. Specifically, we use advanced computational techniques, such as the `Matlab` package `EIG-TOOL`, developed by Wright and Trefethen [23], and the code of Wagenknecht and Agarwal [22], to compute the pseudospectra of first-order systems. In addition, we employ the code of Lancaster and Psarrakos [13] which allows one to compute the pseudospectra of second-order systems which arise from modelling rotating machines. We show how the transients of the full nonlinear system are linked to the transient growth in the linearised system. Furthermore, we investigate the effects which damping and varying initial conditions have on these transients.

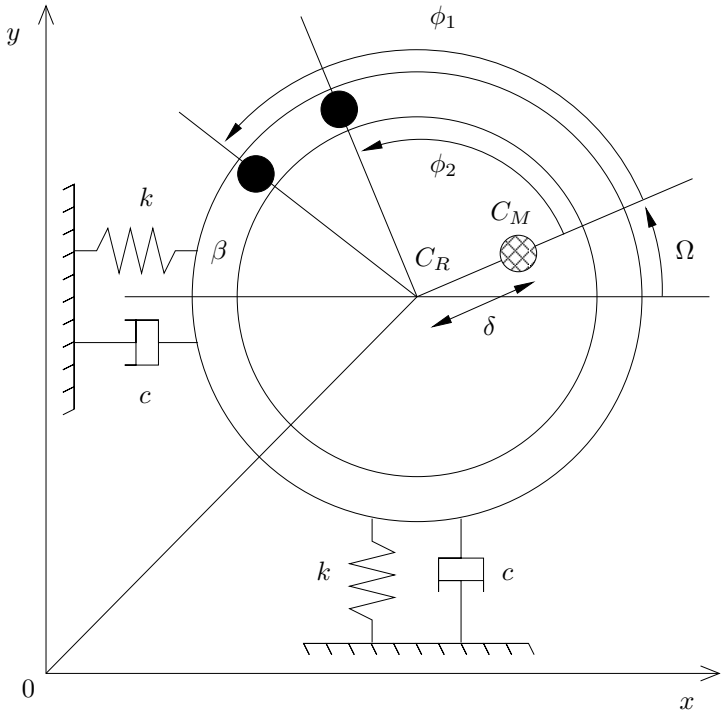


Fig. 1. Schematic diagram of an automatic dynamic balancer with two balancing masses; see the text for definitions of the variables.

In summary, we claim that a linear stability analysis using standard perturbation techniques, and even a full nonlinear bifurcation analysis of steady state solutions is not enough to fully understand the dynamics of the ADB. An analysis and understanding of the sensitivity to perturbation and the ensuing transient response is necessary for a robust design of a widely applicable device.

This paper is organised as follows. In Section 2 we introduce the nonlinear equations of motion modelling the ADB, and in Section 2.1 present their linearisation. In Section 3 we compute the spectrum of the linearisation, and identify a sensitivity of the eigenvalues to perturbation. Furthermore, in Section 4 we compute the pseudospectra of the linearised system and identify which eigenvalues are most sensitive to different forms of structured perturbation. A relationship between this non-normality, sensitivity to perturbation, and the transient dynamics of the ADB is given in Section 5. The effect of damping is considered in Section 6, where we also investigate the effect of varying initial conditions, and Section 7 draws conclusions. Note, all computations are performed using `Matlab`.

## 2 Equations of motion

The equations of motion describing an eccentric rotor fitted with an ADB containing $n$ balancing masses can be written in dimensionless form, in a rotating frame as [1,3,7]

$$\begin{pmatrix} 1+n\mu & 0 \\ 0 & 1+n\mu \end{pmatrix} \begin{pmatrix} \ddot{x} \\ \ddot{y} \end{pmatrix} + \begin{pmatrix} 2\zeta & -2\Omega(1+n\mu) \\ 2\Omega(1+n\mu) & 2\zeta \end{pmatrix} \begin{pmatrix} \dot{x} \\ \dot{y} \end{pmatrix} + \begin{pmatrix} K & -2\Omega\zeta \\ 2\Omega\zeta & K \end{pmatrix} \begin{pmatrix} x \\ y \end{pmatrix} = \begin{pmatrix} \delta\Omega^2 \\ 0 \end{pmatrix} + \mu \sum_{i=1}^{n} \begin{pmatrix} (\Omega+\dot{\phi}_i)^2 & \ddot{\phi}_i \\ -\ddot{\phi}_i & (\Omega+\dot{\phi}_i)^2 \end{pmatrix} \begin{pmatrix} \cos\phi_i \\ \sin\phi_i \end{pmatrix}, \tag{1}$$

and

$$\ddot{\phi}_i + \beta\dot{\phi}_i = (\ddot{x} - \Omega^2 x - 2\Omega\dot{y})\sin\phi_i - (\ddot{y} - \Omega^2 y + 2\Omega\dot{x})\cos\phi_i, \quad i = 1, .., n \tag{2}$$

where dimensionless state variables describe the displacement due to radial vibration in the $x \equiv x(t)$ and $y \equiv y(t)$ directions, and the angular position $\phi_i \equiv \phi_i(t)$ of $i$th ball, with respect to the imbalance. This set-up is shown schematically in Fig. 1. Dimensionless parameters describe the mass ratio $\mu$ between a single ball and the rotor system, the external damping ratio (between linear damping coefficients $c$ and linear spring constants $k$) of the system $\zeta$, the angular velocity of the rotor $\Omega$, the eccentricity or distance of the centre of mass from the centre of rotation $\delta$, and the internal viscous damping of the balls in the balancer $\beta$. Without loss of generality, all parameters are assumed to be positive. Furthermore, $K = 1 - \Omega^2(1 + n\mu)$; see Ref. [7] for full details. Theoretical studies, where the ADB is modelled using equations similar to (1) and (2), can be found in Refs. [1–3,14,15,17]. Similarly, experimental results can be found in Refs. [14,18]. For this study we focus on the case with only two balancing masses, that is, $n = 2$.

### *2.1 Linearisation about the balanced steady state*

For fixed parameters, a balanced steady state of (1) and (2) is given by

$$
\begin{aligned}
&x^s = y^s = 0,\\
&\phi_1^s = \arccos\left(-\frac{\delta}{2\mu}\right),\\
&\phi_2^s = -\phi_1^s.
\end{aligned}
\tag{3}
$$

In other words, the centre of the mass of the system is located at the centre of rotation. By linearising about this balanced state, (1) and (2) can be written in the following form

$$
A_2\ddot{\mathbf{x}} + A_1\dot{\mathbf{x}} + A_0\mathbf{x} = 0 \tag{4}
$$

where $\mathbf{x} = (x, y, \phi_1, \phi_2)(t)$, and the Jacobian matrices are given by

$$
A_2 = \begin{pmatrix}
1+2\mu & 0 & -\mu\sin(\phi_1^s) & -\mu\sin(\phi_2^s)\\
0 & 1+2\mu & \mu\cos(\phi_1^s) & \mu\cos(\phi_2^s)\\
-\sin(\phi_1^s) & -\cos(\phi_1^s) & 1 & 0\\
-\sin(\phi_2^s) & -\cos(\phi_2^s) & 0 & 1
\end{pmatrix}, \tag{5}
$$

$$
A_1 = \begin{pmatrix}
2\zeta & -2\Omega(1+2\mu) & -2\mu\Omega\cos(\phi_1^s) & -2\mu\Omega\cos(\phi_2^s)\\
2\Omega(1+2\mu) & 2\zeta & -2\mu\Omega\sin(\phi_1^s) & -2\mu\Omega\sin(\phi_2^s)\\
2\Omega\cos(\phi_1^s) & 2\Omega\sin(\phi_1^s) & \beta & 0\\
2\Omega\cos(\phi_2^s) & 2\Omega\sin(\phi_2^s) & 0 & \beta
\end{pmatrix}, \tag{6}
$$

and

$$
A_0 = \begin{pmatrix}
K & -2\Omega\zeta & \mu\Omega^2\sin(\phi_1^s) & \mu\Omega^2\sin(\phi_2^s)\\
2\Omega\zeta & K & -\mu\Omega^2\cos(\phi_1^s) & -\mu\Omega^2\cos(\phi_2^s)\\
\Omega^2\sin(\phi_1^s) & -\Omega^2\cos(\phi_1^s) & \Omega^2(x^s\cos(\phi_1^s) + y^s\sin(\phi_1^s)) & 0\\
\Omega^2\sin(\phi_2^s) & -\Omega^2\cos(\phi_2^s) & 0 & \Omega^2(x^s\cos(\phi_2^s) + y^s\sin(\phi_2^s))
\end{pmatrix}. \tag{7}
$$

In this way the matrices $A_2$, $A_1$, and $A_0$ can be termed the mass, damping, and stiffness matrices, respectively.

Alternatively, (4) can be written as the first-order linear system

$$
\dot{\mathbf{z}} = \mathcal{A}\mathbf{z}, \tag{8}
$$

where $\mathbf{z} = (\mathbf{x}, \dot{\mathbf{x}}) \equiv (x, y, \phi_1, \phi_2, \dot{x}, \dot{y}, \dot{\phi}_1, \dot{\phi}_2)(t)$, and

$$\mathcal{A} = \begin{pmatrix} 0 & I \\ -A_2^{-1}A_0 & -A_2^{-1}A_1 \end{pmatrix}. \tag{9}$$

In (9), 0 is the null matrix and $I$ is the identity matrix.

## 3 Stability and sensitivity to perturbation

From here on in, unless otherwise stated, we will consider the fixed parameter set

$$\Omega = 5.0,\ \zeta = 0.01,\ \beta = 0.01,\ \delta = 0.01,\ \mu = 0.05. \tag{10}$$

For these parameters, a stable balanced steady state exists and is given by (3) as

$$(x^s, y^s, \phi_1^s, \phi_2^s) = (0, 0, 1.67096 + 2n\pi, -1.67096 + 2n\pi), \quad n \in \mathbb{Z}, \tag{11}$$

where time derivatives are set to zero. Therefore, for the parameter set (10) the matrix $\mathcal{A}$ given by (9) becomes

$$\mathcal{A} = \begin{pmatrix} 0 & 0 & 0 & 0 & 1.0000 & 0 & 0 & 0 \\ 0 & 0 & 0 & 0 & 0 & 1.0000 & 0 & 0 \\ 0 & 0 & 0 & 0 & 0 & 0 & 1.0000 & 0 \\ 0 & 0 & 0 & 0 & 0 & 0 & 0 & 1.0000 \\ 24.0010 & 0.0999 & -1.2425 & 1.2425 & -0.0200 & 10.0000 & -0.0504 & -0.0495 \\ -0.0910 & 24.0901 & -0.1137 & -0.1137 & -10.0000 & -0.0182 & 0.4526 & -0.4527 \\ -1.0031 & 0.0084 & -1.2476 & 1.2249 & -0.0199 & -0.0018 & -0.0149 & -0.0945 \\ 0.9849 & -0.1904 & 1.2249 & -1.2476 & 0.0199 & -0.0018 & 0.0955 & -0.0061 \end{pmatrix}. \tag{12}$$

By solving the linear eigenvalue problem

$$(\mathcal{A} - \lambda I)\mathbf{v} = 0, \tag{13}$$

the spectrum $\Lambda$ of $\mathcal{A}$ is easily computed to be

$$\Lambda = \left\{ \begin{array}{c} -0.0091 \pm 5.9541i,\ -0.0092 \pm 4.0450i, \\ -0.0064 \pm 1.6051i,\ -0.0050 \pm 0.1533i \end{array} \right\}. \tag{14}$$

We will refer to these four complex-conjugate pairs of eigenvalues as $\{\lambda_1^{\pm}, \lambda_2^{\pm}, \lambda_3^{\pm}, \lambda_4^{\pm}\}$, where $|\Im(\lambda_1^{\pm})| > |\Im(\lambda_2^{\pm})| > |\Im(\lambda_3^{\pm})| > |\Im(\lambda_4^{\pm})|$. The corresponding right eigenvectors of (14) are

$$\mathbf{v} = \begin{pmatrix} -0.0002 \mp 0.1172i & -0.0004 \mp 0.1698i & 0.0018 \mp 0.0354i & 0.0000 \mp 0.0004i \\ 0.1169 \mp 0.0002i & 0.1687 \mp 0.0004i & 0.0009 \mp 0.0001i & 0.0066 \pm 0.0000i \\ 0.0003 \mp 0.0035i & 0.0004 \mp 0.0121i & -0.0015 \mp 0.3732i & 0.6993 \\ 0.0002 \pm 0.0035i & 0.0009 \pm 0.0121i & -0.0408 \pm 0.3707i & 0.6985 \pm 0.0084i \\ 0.6980 & 0.6869 & 0.0569 \pm 0.0031i & 0.0001 \pm 0.0000i \\ 0.0000 \pm 0.6961i & -0.0001 \pm 0.6824i & 0.0002 \pm 0.0014i & -0.0000 \pm 0.0010i \\ 0.0210 \pm 0.0018i & 0.0491 \pm 0.0017i & 0.5991 & -0.0035 \pm 0.1072i \\ -0.0210 \pm 0.0011i & -0.0490 \pm 0.0037i & -0.5947 \mp 0.0678i & -0.0047 \pm 0.1070i \end{pmatrix}. \tag{15}$$

The first two columns of $\mathbf{v}$, corresponding to the first two eigenvalues $\lambda_1^{\pm}$ and $\lambda_2^{\pm}$ of $\Lambda$, can be seen to have dominant components in the first, second, fifth and sixth rows. Likewise, the last two columns of $\mathbf{v}$, corresponding to the last two eigenvalues $\lambda_3^{\pm}$ and $\lambda_4^{\pm}$ of $\Lambda$, are shown to have dominant components in the third, fourth, seventh and eighth rows. Physically, this means that we can associate the first two eigenvalues $\lambda_1^{\pm}$ and $\lambda_2^{\pm}$ (those with large imaginary part) to the motion of the rotor ($x$, $y$), and the last two eigenvalues $\lambda_3^{\pm}$ and $\lambda_4^{\pm}$ (those with smaller imaginary part) to the motion of the balls ($\phi_1$, $\phi_2$). In other words, the rotor responds at a high frequency and the balls at a lower frequency.

It can be seen that some elements of (12) have relatively large real part; for example, see row five, column one. This is an indication that the eigenvalue problem is ill-conditioned, that is, the eigenvalues are highly sensitive to perturbation; small changes in the elements of $\mathcal{A}$ can produce large changes in the eigenvalues. This is also evident in the fact that the first two eigenvectors of (15) point in similar directions, that is, they are far from being orthogonal and, hence, $\mathcal{A}$ is highly non-normal.

One such measure of normality $\hat{n}$ of a matrix $M$ can be written as [20]

$$\hat{n} = \frac{\|M^H M - M M^H\|}{\|M\|^2}, \tag{16}$$

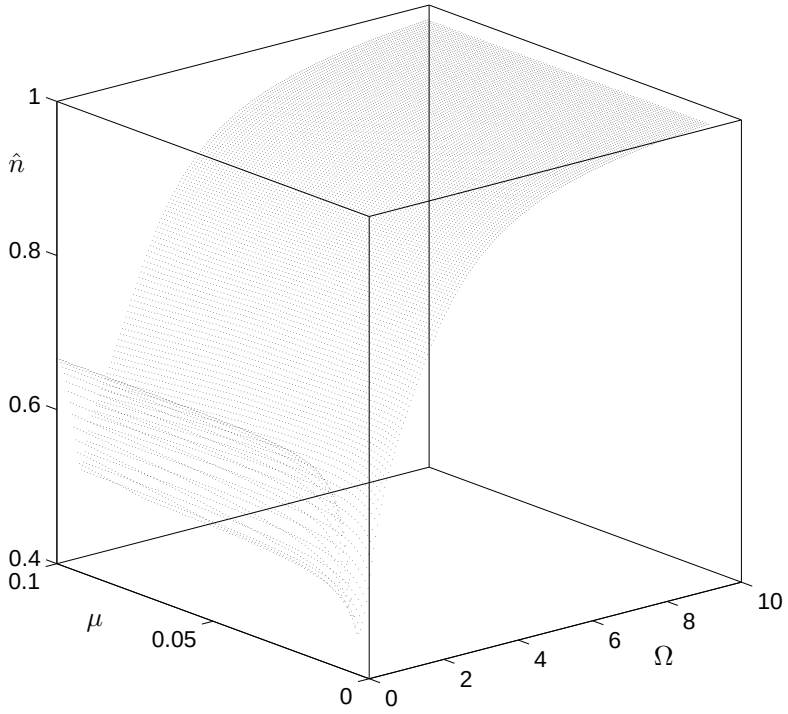


Fig. 2. Normality $\hat{n}$ of the matrix $\mathcal{A}$, given by (12), over the ($\Omega$, $\mu$)-plane; other parameters were fixed at $\zeta = \beta = \delta = 0.01$.

where $M^H$ is the conjugate transpose of the matrix $M$ (which in the case of a real matrix is just its transpose). For a normal matrix, $M^H M = M M^H$ and, therefore, $\hat{n} = 0$.

Figure 2 shows the normality of the matrix $\mathcal{A}$, given by (9), over the ($\Omega$, $\mu$)-parameter plane. It is shown that as the rotational speed $\Omega$ is increased the matrix $\mathcal{A}$ becomes increasingly non-normal; all other parameters were fixed at the values (10). Again, this result is associated with the large elements of (12) (row five, column one and row six, column two). These elements are dominated by the term $-K \approx (\Omega^2 - 1)$. Physically, $K$ represents the effect of centripetal acceleration. It is often called 'spin softening' or 'centripetal softening' because it reduces the effective stiffness of the system.

Stability information can also be found by considering the linearisation (4). In this case we solve the quadratic eigenvalue problem given by [12]

$$Q(\lambda)\mathbf{w} = (\lambda^2 A_2 + \lambda A_1 + A_0)\mathbf{w} = 0. \tag{17}$$

We will consider the matrix polynomial $Q(\lambda)$ later. For now, we note that the eigenvalues $\lambda$ of (17) are identical to those given in (14), and also

$$\mathbf{v} = \left\{ \begin{array}{c} \mathbf{w} \\ \lambda \mathbf{w} \end{array} \right\}. \tag{18}$$

## 4 Pseudospectra

An important concept in identifying the sensitivity of eigenvalues to perturbation is that of pseudospectra [20]. In the complex plane, the $\epsilon$-pseudospectrum of a matrix $\mathcal{A}$ is a compact subset containing one or more of the eigenvalues. This subset consists of all possible locations of the eigenvalues of the matrix $\mathcal{A}$ when it is perturbed by a random perturbation matrix $E$ of norm less than $\epsilon$. The pseudospectrum of a non-normal matrix extends into a larger area of the complex plane than that of a normal matrix; in the latter case, the pseudospectra are simply concentric circles around the eigenvalues. In other words, for a non-normal matrix, small perturbations can lead to large changes in the possible locations of the eigenvalues. We define the eigenvalue most sensitive to perturbation to be the one whose pseudospectrum reaches the right-half plane for the smallest value of $\epsilon$.

For the linear eigenvalue problem (13) the $\epsilon$-pseudospectrum [20] is given by

$$\Lambda_\epsilon(\mathcal{A}) = \{z \in \mathbb{C} : z \in \Lambda(\mathcal{A} + E) \text{ for some } E \text{ with } \|E\| \leq \epsilon\} \tag{19}$$

$$= \{\lambda \in \mathbb{C} : \|(\lambda I - \mathcal{A})^{-1}\| \geq \epsilon^{-1}\}. \tag{20}$$

where $\Lambda$ denotes the spectrum.

Figure 3 shows $\epsilon$-pseudospectra of the linearisation (9) of (1) and (2) computed using the `Matlab` package `EIG-TOOL` [23]. In Fig. 3(a) we show constant contours centred around the four eigenvalues $\lambda_i^-$ $(i = 1..4)$, indicated by the large black dots (the remaining four eigenvalues $\lambda_i^+$ $(i = 1..4)$ and their associated contours are obtained by applying symmetry about the $\Im(z) = 0$ axis). From outermost to innermost, the contours correspond to pseudospectrum with $\epsilon = 10^{-1}$, $10^{-1.5}$, $10^{-2}$, and $10^{-2.5}$ (the $10^{-2.5}$ contour may be very close to the eigenvalue and, therefore, not always visible). Figure 3(b) shows a zoom of the pseudospectra of the eigenvalue most sensitive to perturbation, $\lambda_1^\pm = -0.0091 \pm 5.9541i$, and this is also the eigenvalue with the largest imaginary part (in magnitude). In this case, from outermost to innermost, the contours correspond to pseudospectra with $\epsilon = 10^{-3}$, $10^{-3.5}$, $10^{-4}$, and $10^{-4.5}$. It is clear that a perturbation of $\epsilon > 10^{-3}$ is enough to potentially destabilise the system. Physically, $\lambda_1^\pm$ is associated with a high frequency response of the motion of the rotor.

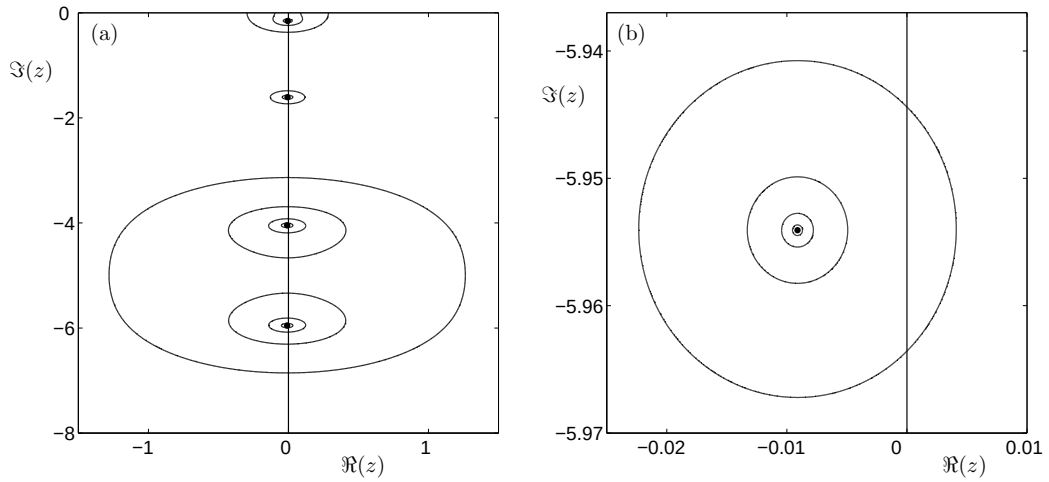


Fig. 3. Pseudospectra of a balanced steady state solution Panel (a) shows the $\epsilon$-pseudospectra of the linear eigenvalue problem $\Lambda_\epsilon(\mathcal{A})$. From outermost to innermost, the contours correspond to $\epsilon$-pseudospectra with $\epsilon = 10^{-1}, 10^{-1.5}, 10^{-2}$, and $10^{-2.5}$. Panel (b) shows the $\epsilon$-pseudospectra of the eigenvalue most sensitive to perturbation. From outermost to innermost, the contours correspond to pseudospectra with $\epsilon = 10^{-3}, 10^{-3.5}, 10^{-4}$, and $10^{-4.5}$. For fixed parameters given by (10).

### *4.1 Structured perturbation*

In practical usage, one may wish to investigate the effect of a structured perturbation, that is, instead of a random perturbation applied to the entire system, perturbations are applied to pre-specified elements of the governing matrix. This can be of particular importance when the elements of the matrix represent different physical properties with different magnitudes. In our case, we briefly investigate the effect of applying structured perturbations to different combinations of the mass $A_2$, damping $A_1$ and stiffness $A_0$ matrices.

Our first structured perturbation is applied to the first-order linearisation (9). The method we employ was developed by Wagenknecht and Agarwal [22]. It allows one to apply weighted perturbations to individual elements of a matrix $\mathcal{A}$. Specifically, the $\epsilon$-pseudospectrum of the matrix $\mathcal{A}$ is defined as

$$\Lambda_\epsilon(\mathcal{A}) = \left\{ \begin{array}{c} z \in \mathbb{C} : z \in \Lambda\left(\mathcal{A} + \sum_{i=1}^{n}\sum_{j=1}^{n} W_{ij} \cdot P_{ij} \cdot e_i e_j^T\right) \\ \text{for some } P \text{ with } \max(P_{ij}) < \epsilon \end{array} \right\}, \tag{21}$$

where $n$ is the dimension of $\mathcal{A}$, $W = (W_{ij})$ is a weight matrix, $P$ is an arbitrary perturbation matrix, and $(e_i)$ is a vector of zeros except for the $i$th element which takes the value of unity; see Ref. [22] for full details.

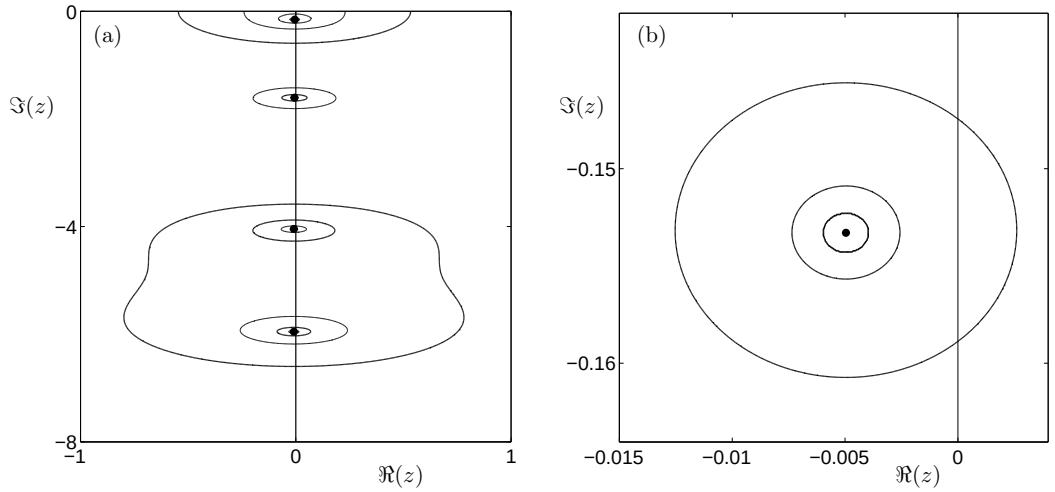


Fig. 4. Structured pseudospectra of a balanced steady state solution. Panel (a) shows the pseudospectra of the linear eigenvalue problem $\Lambda_\epsilon(\mathcal{A})$ with perturbations applied to the lower half of $\mathcal{A}$. From outermost to innermost, the contours shown in the first column correspond to pseudospectra with $\epsilon = 10^{-1}$, $10^{-1.5}$, $10^{-2}$, and $10^{-2.5}$. Panel (b) shows the pseudospectra of the eigenvalue most sensitive to perturbation. From outermost to innermost, the contours correspond to pseudospectra with $\epsilon = 10^{-3}$, $10^{-3.5}$, $10^{-4}$, and $10^{-4.5}$. For fixed parameters given by (10).

Figure 4 was computed by applying perturbations with weight elements of size unity to all elements of the two lower sub-matrices $(-A_2^{-1}A_0)$ and $(-A_2^{-1}A_1)$ of (9). From outermost to innermost, the contours in Fig. 4(a) correspond to pseudospectra with $\epsilon = 10^{-1}$, $10^{-1.5}$, $10^{-2}$, and $10^{-2.5}$. It can be seen that by using this form of *block perturbation* the eigenvalue $\lambda_4^{\pm}$ closest to the $\Im(z) = 0$ axis is now the one most sensitive to perturbation. Physically, $\lambda_4^{\pm}$ is associated with the low frequency response of the motion of the balls. In fact, the pseudospectra of the eigenvalue $\lambda_4^{\pm}$ is shown to extend into the right-half plane nearly as far as the pseudospectra of the eigenvalues with large imaginary part $\lambda_1^{\pm}$ and $\lambda_2^{\pm}$ (rotor modes). This is in stark contrast to Fig. 3. Figure 4(b) shows a zoom of the pseudospectrum of $\lambda_4^{\pm}$. From outermost to innermost, the contours correspond to pseudospectra with $\epsilon = 10^{-3}$, $10^{-3.5}$, $10^{-4}$, and $10^{-4.5}$. It is seen that a perturbation of $\epsilon > 10^{-3}$ is enough to potentially destabilise the system. Note that, in Fig. 4(b), the pseudospectra for $\epsilon = 10^{-4}$ and $10^{-4.5}$ are almost identical and hence only three contours are visible. We note that the eigenvalue $\lambda_1^{\pm}$, furthest from the $\Im(z) = 0$ axis and the one shown to be most sensitive to perturbation in Fig. 3, is the next most sensitive.

Our second structured perturbation is applied to the second-order system (4). In this case, one introduces a perturbation matrix $\Delta(\lambda)$ to the quadratic polynomial $Q(\lambda)$ (see (17)) such that

$$\Delta(\lambda) = \lambda^2\Delta_2 + \lambda\Delta_1 + \Delta_0. \tag{22}$$

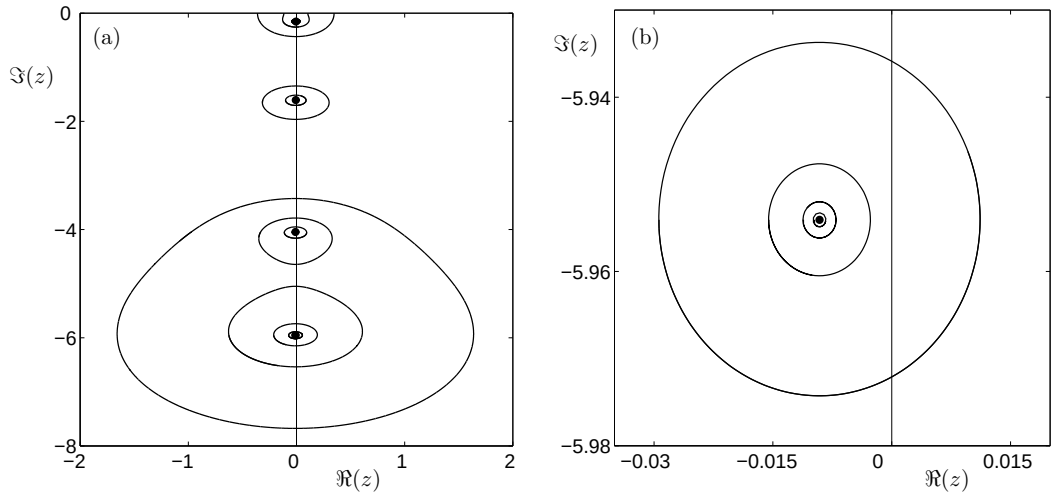


Fig. 5. Structured pseudospectra of a balanced steady state solution. Panel (a) shows the $\epsilon$-pseudospectra of the quadratic eigenvalue problem $\Lambda_\epsilon(Q)$ with absolute weights $w_i = 1$. From outermost to innermost, the contours shown in the first column correspond to $\epsilon$-pseudospectra with $\epsilon = 10^{-1}, 10^{-1.5}, 10^{-2}, 10^{-2.5}$, and $10^{-3}$. Panel (b) shows the $\epsilon$-pseudospectra of the eigenvalue most sensitive to perturbation. From outermost to innermost, the contours correspond to pseudospectra with $\epsilon = 10^{-3}, 10^{-3.5}, 10^{-4}$, and $10^{-4.5}$. For fixed parameters given by (10).

The $\epsilon$-pseudospectra of $Q$ is defined as

$$\Lambda_\epsilon(Q) = \left\{ \begin{array}{c} \lambda \in \mathbb{C} : (Q(\lambda) + \Delta(\lambda))\mathbf{w} = 0 \text{ for some } \mathbf{w} \neq 0 \\ \text{and } \Delta(\lambda) \text{ with } \|\Delta_k\| \leq \epsilon w_k,\ k = 0, 1, 2 \end{array} \right\}. \tag{23}$$

The weight parameters $w_k$ allow one to decide how the perturbations are applied; for example, an absolute perturbation $w_k \equiv 1$, or a relative perturbation $w_k = \|A_k\|$ [13,19].

Figure 5 was computed using the numerical method described by Lancaster and Psarrakos [13]. Shown is the $\epsilon$-pseudospectra of the second-order system given by (4) with absolute perturbations, that is, $w_k \equiv 1$; see (23). From outermost to innermost, the contours in Fig. 5(a) correspond to pseudospectra with $\epsilon = 10^{-1}, 10^{-1.5}, 10^{-2}$, and $10^{-2.5}$. Figure 5(b) shows a zoom of the most sensitive eigenvalue $\lambda_1^{\pm}$. From outermost to innermost, the contours correspond to pseudospectra with $\epsilon = 10^{-3}, 10^{-3.5}, 10^{-4}$, and $10^{-4.5}$. As was the case for Fig. 3, it is clear that a perturbation of $\epsilon > 10^{-3}$ is enough to potentially destabilise the system. In this case, the $\epsilon$-pseudospectrum of the linearised system (9) gives the same information as for the quadratic eigenvalue problem obtained from the linearisation of the second-order system (4); see Fig. 3. Both reveal the eigenvalue $\lambda_1^{\pm}$ (a rotor mode) to be most sensitive to perturbation. However, note that the $\epsilon = 10^{-3}$ contour in Fig. 5(b) stretches further into

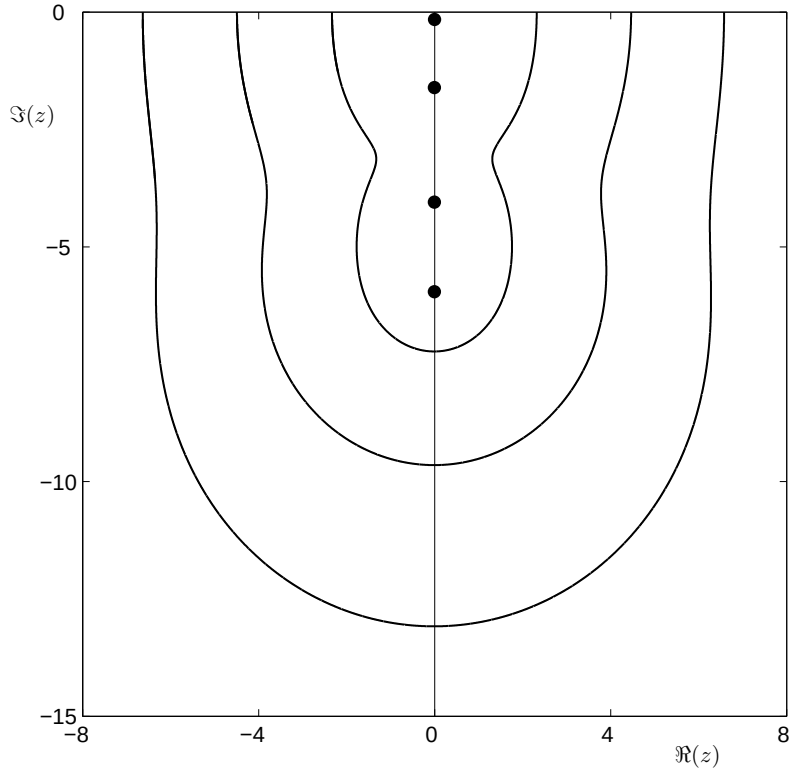


Fig. 6. Pseudospectra of a balanced steady state solution showing the effect of structured perturbations of the quadratic eigenvalue problem $\Lambda_\epsilon(Q)$ for $\epsilon = 10^{-1}$. The outermost contour corresponds to weights $w_k = \|A_k\|$, $k = 0, 1, 2$; the next contour corresponds to weights $w_{0,1} = \|A_{0,1}\|$, $w_2 = 0$; and the innermost contour corresponds to weights $w_0 = \|A_0\|$, $w_{1,2} = 0$. For fixed parameters given by (10).

the right-half plane $\Re(z) > 0$ than the $\epsilon = 10^{-3}$ contour of Fig. 3(b).

Figure 6 was also computed using the numerical method described in Ref. [13]. Shown is the $\epsilon = 10^{-1}$ pseudospectra of the second-order system given by (4) for three different weighted perturbations. The outermost contour shows the case of relative perturbations, that is, $w_k = \|A_k\|$. Specifically, for the parameter set (10), $w_0 = 44.05543$, $w_1 = 17.86064$ and $w_2 = 1.98511$. The next contour shows the same relative perturbations applied to the stiffness $A_0$ and damping $A_1$ matrices but with the weight $w_2$, associated with the mass matrix $A_2$, set to zero. The innermost contour again shows a relative perturbation applied to the matrix $A_0$ but with both the weights $w_1$ and $w_2$ applied to the respective matrices $A_1$ and $A_2$ set to zero. It is apparent from Fig. 6 that the eigenvalue $\lambda_4^{\pm}$, closest to the $\Im(z) = 0$ axis, is now most sensitive to perturbation. This is in contrast to the case of an absolute perturbation (Fig. 5) where the eigenvalue $\lambda_1^{\pm}$, furthest from the $\Im(z) = 0$ axis, was shown to be most sensitive to perturbation. However, this last result of applying a perturbation to the $A_0$ matrix only, does agree with the block perturbation method used to produce Fig. 4.

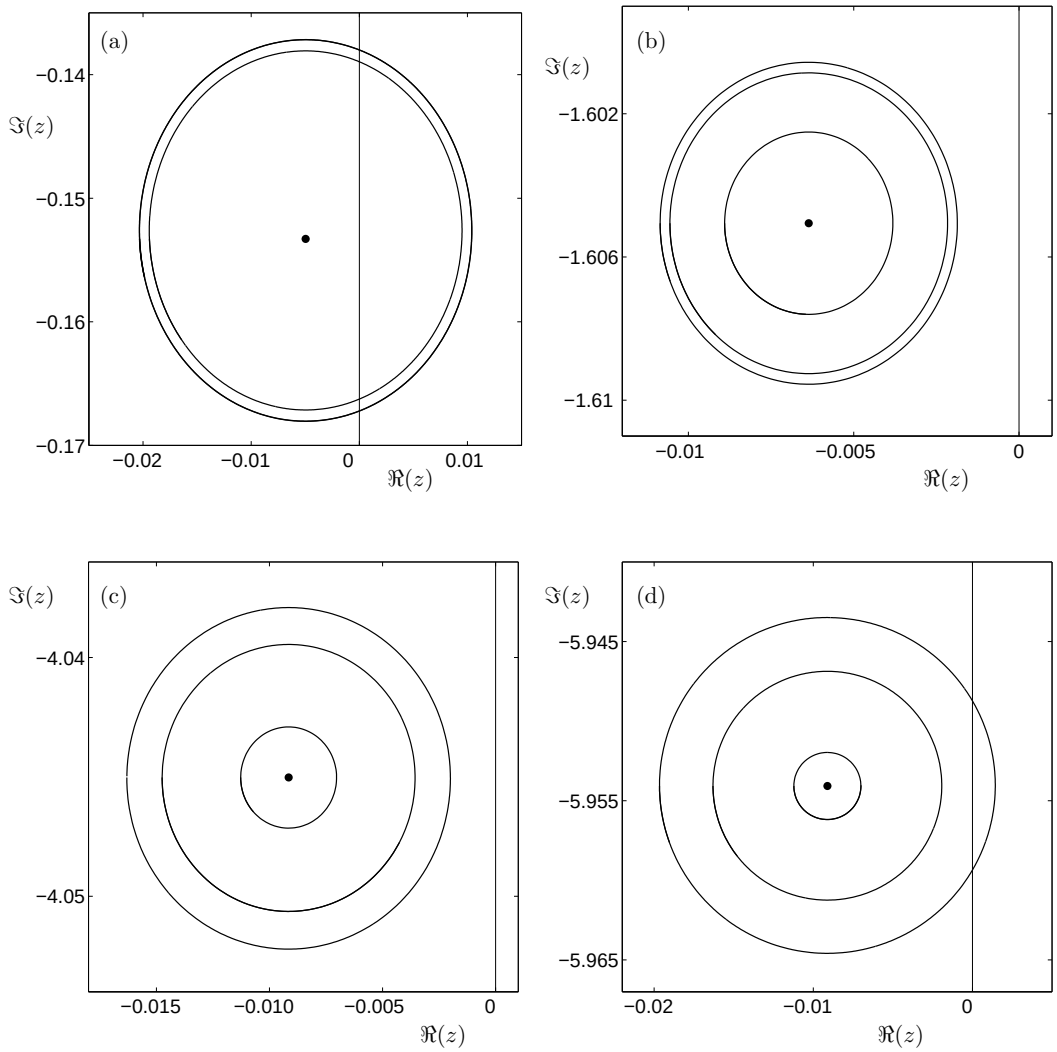


Fig. 7. Pseudospectra of a balanced steady state solution showing the effect of structured perturbations of the quadratic eigenvalue problem $\Lambda_\epsilon(Q)$ for $\epsilon = 10^{-4}$. In each panel, the outermost contour corresponds to weights $w_k = \|A_k\|$, $k = 0, 1, 2$; the next contour corresponds to weights $w_{0,1} = \|A_{0,1}\|$, $w_2 = 0$; and the innermost contour corresponds to weights $w_0 = \|A_0\|$, $w_{1,2} = 0$. For fixed parameters given by (10).

Figure 7 shows the $\epsilon = 10^{-4}$ pseudospectra of the second-order system given by (4) for the different weighted perturbations used to compute Fig. 6, detailed above. Figures 7(a) to (d) show the pseudospectra about the eigenvalues $\lambda_4^\pm$, $\lambda_3^\pm$, $\lambda_2^\pm$, and $\lambda_1^\pm$, given by (14), respectively. Note that in Fig. 7(a) the pseudospectra for the first two weighted perturbations are almost identical and hence only two contours are visible. It is now clear that the eigenvalue $\lambda_4^\pm$, closest to the $\Im(z) = 0$ axis, is most sensitive to structured perturbations. In fact, the only other potentially destabilising perturbation is shown in Fig. 7(d) and corresponds to the $w_k = \|A_k\|$ perturbation weighting applied to the eigen-

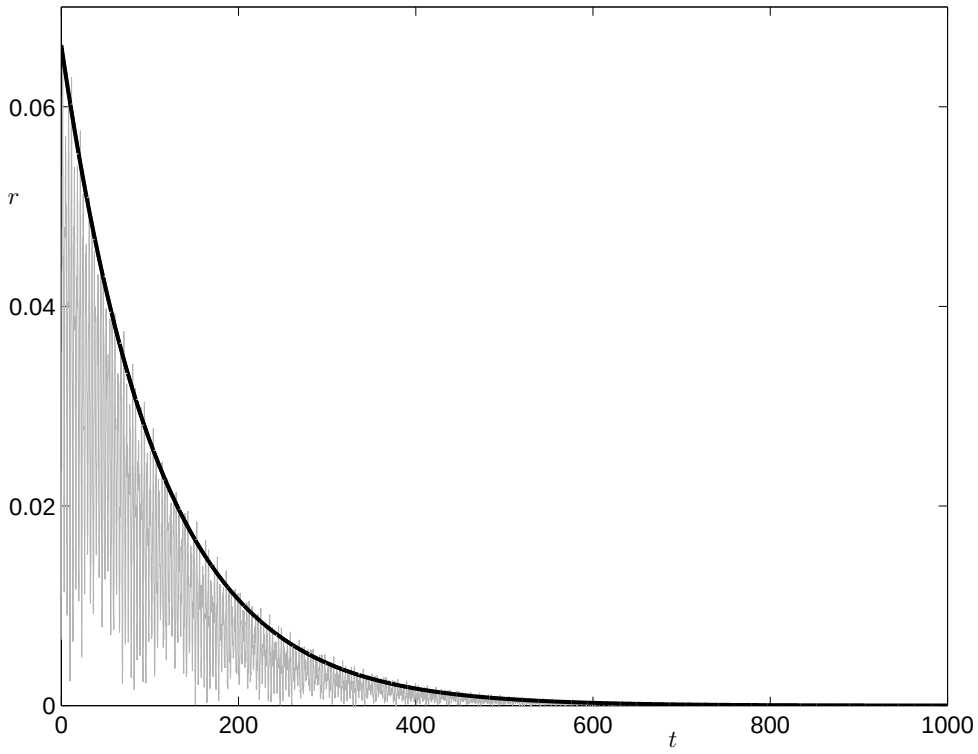


Fig. 8. Transient of the magnitude of the radial vibration $r$ for the parameter set given by (10). Initial conditions were fixed at $x = y = \dot{x} = \dot{y} = \dot{\phi}_1 = \dot{\phi}_2 = 0$, $\phi_1 = -\pi/2$, and $\phi_2 = \pi/2$. The thick curve represents to the decay rate of the leftmost eigenvalue.

value $\lambda_1^{\pm}$, furthest from the $\Im(z) = 0$ axis. Again, this last observation agrees with the block perturbation of Fig. 4.

In summary, if we only consider random perturbations to the matrix $\mathcal{A}$, viewing the problem as an eight-dimensional system with no structure, the effect of perturbation is most likely to be seen in the motion of the rotor (modes corresponding to $\lambda_1^{\pm}$ and $\lambda_2^{\pm}$). However, when taking into account the physics of the problem and applying structured perturbations to the mass, damping, and stiffness matrices, we find that the order of which eigenvalues are most sensitive to perturbation can change. In particular, applying perturbations to the stiffness matrix only, it was shown that the effect of perturbation was most likely to be seen in the motion of the balls (modes corresponding to $\lambda_3^{\pm}$ and $\lambda_4^{\pm}$). We now test which of the above scenarios is observed in numerical simulation of the full nonlinear equations of motion (1) and (2).

## 5 Transient behaviour and the matrix exponential

The ADB is known to undergo long intervals of transient vibration before a balanced equilibrium is reached. Figure 8 shows a typical transient for the parameter set (10), and for the initial conditions $x = y = \dot{x} = \dot{y} = \dot{\phi}_1 = \dot{\phi}_2 = 0$, $\phi_1 = -\pi/2$, and $\phi_2 = \pi/2$, that is, the balls are launched from rest within the rotating frame, from opposite positions on an axis orthogonal to the direction of the imbalance. Alternatively, this initial condition can be thought of as a small perturbation applied to the position of the balls from the steady state (11). In the figure, the magnitude of the radial displacement $r = \sqrt{(x^2 + y^2)}$ is plotted against the dimensionless time $t$. For all numerical integration we used the `Matlab` routine `ode45`.

Observe from Fig. 8 that the trajectory of the full nonlinear system (1) and (2) instantly increases to $r \approx 0.066$ from its initially zero radial displacement. This is followed by a high frequency, exponential decay to the balanced state such that $r < 10^{-4}$ at $t = 700$. Appealing to intuition from normal mode theory, one would expect the decay rate to initially be determined by the real part of the leftmost eigenvalue, before quickly being drawn to and decaying at a rate determined by the real part of the next leftmost, and so on. Subsequently, and for the most part, one would expect to observe asymptotic decay determined by the real part of the rightmost eigenvalue. However, interestingly, the exponential decay of the transient is shown to follow the strong stable manifold associated with the leftmost eigenvalue $\lambda_L \equiv \lambda_1^{\pm} = -0.0091 \pm 5.9541i$ (a rotor mode), as indicated by the thick curve defined by $f_1(t) = \max(r)\mathrm{e}^{\Re(\lambda_L)t}$, for its entire duration.

We claim that this transient behaviour can be explained in terms of the non-normality of the linearised system describing the ADB. Recall that, for a normal matrix $A$ and assuming stability, $\|\mathrm{e}^{At}\|$ decreases monotonically for $t > 0$. However, if the matrix $A$ is non-normal one may expect transient growth in this matrix exponential before eventual decay.

Figure 9 clearly shows this transient growth in the matrix exponential of the linearised system (9) and the ensuing decay. In each panel the evolution of $\|\mathrm{e}^{\mathcal{A}t}\|$ is shown as a grey trajectory, along with a dashed black curve defined by $f_2(t) = \mathrm{e}^{\Re(\lambda_R)t}$, and a solid black curve defined by $f_3(t) = \max(\|\mathrm{e}^{\mathcal{A}t}\|)\mathrm{e}^{\Re(\lambda_L)t}$. Figure 9(a) clearly shows initial transient growth in $\|\mathrm{e}^{\mathcal{A}t}\|$. The transient is then shown to decay at a rate determined by the leftmost eigenvalue $\lambda_L$; see Figs. 9(a) and (b). It was shown in Sec. 4 (and Fig. 3) that this eigenvalue is most sensitive to perturbation. A lower bound on the size of the initial transient growth can be found by considering the pseudospectra of this eigenvalue: the matrix exponential $\|\mathrm{e}^{\mathcal{A}t}\|$ must be greater than $\eta/\epsilon$ for some $t > 0$, where the $\epsilon$-pseudospectra extends a distance $\eta$ into the right-half plane [8,20]. In

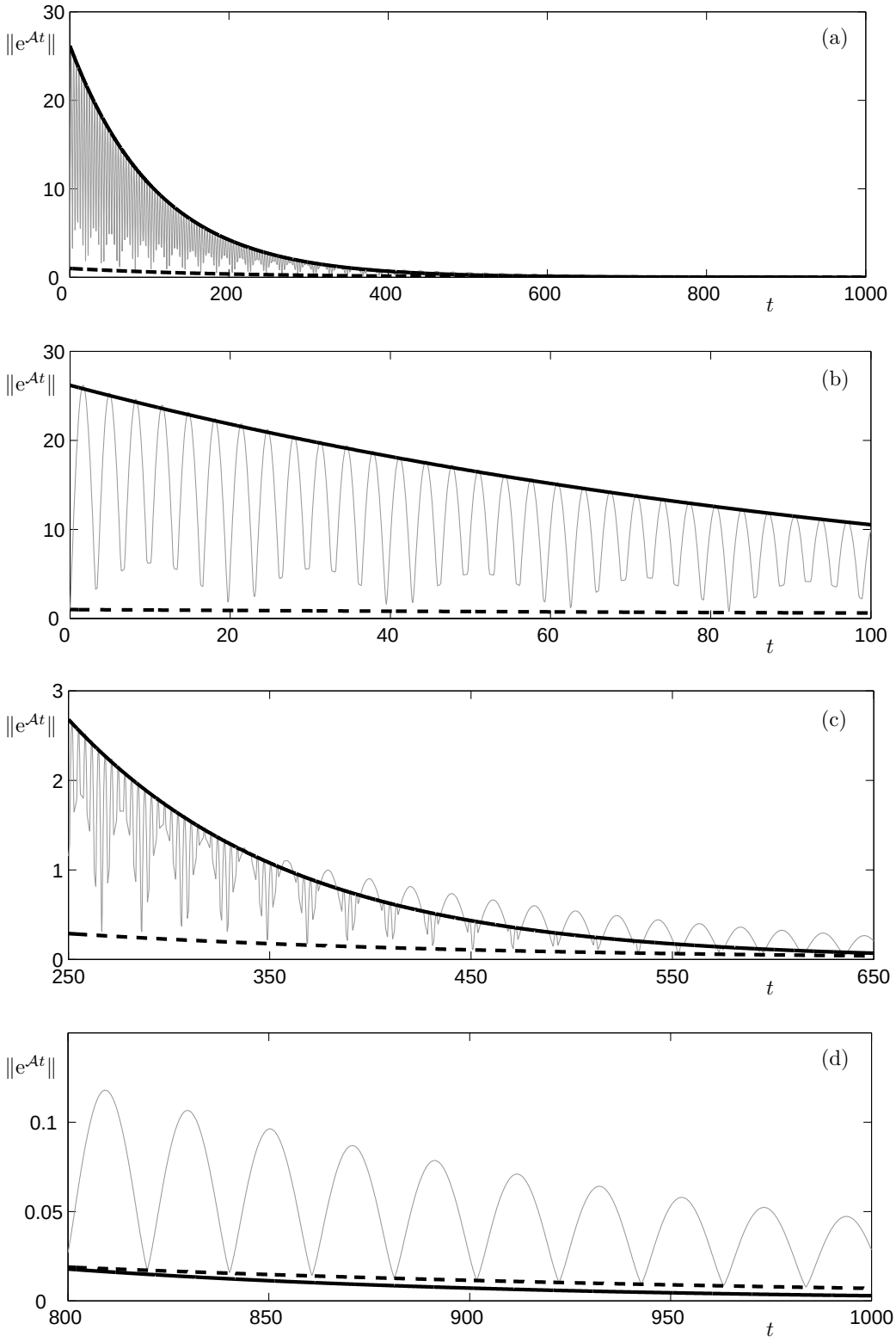


Fig. 9. Transient behaviour of the matrix exponential $\|e^{At}\|$. For fixed parameters given by (10). The solid curve represents the decay rate of the leftmost eigenvalue and the dashed curve the decay rate of the rightmost eigenvalue.

our case, this measure is calculated to be 12.63 when the $\epsilon = 10^{-1}$ contour of Fig. 3(a) was considered. The frequency of the oscillation of this initial decay is determined by the large imaginary part of this leftmost eigenvalue $\lambda_L$ (a rotor mode). Note that these fast oscillations can be seen to occur in slowly oscillating 'packets' on the frequency of the rightmost eigenvalue $\lambda_R$ (a ball mode), with a small imaginary part. Figure 9(c) shows that at $t \approx 350$ this slow oscillation starts to dominate and the fast oscillations are destroyed. Eventually, as expected the transient decays along the dashed curve determined by the rightmost eigenvalue $\lambda_R$; see Fig. 9(d).

### *5.1 Transient response near the critical rotation speed*

In Ref. [7] it was shown that the ADB can achieve balance close to the critical rotation speed $\Omega = 1$; the rotation speed at which one observes greatest radial vibration in the standard eccentric rotor model. This region of stability was found to be in the shape of a thin wedge of parameter space bounded by oscillatory, Hopf instabilities. We now briefly digress from considering the parameter set (10) and investigate the transient response of a perturbation to this balanced state close to the critical rotation speed.

Figures 10(a) and (b) show the pseudospectra of the balanced steady state inside this wedge for the parameter set (10) but with $\Omega = 1.04$. For these parameters, the eigenvalues of the balanced steady state are given as

$$\Lambda = \{-0.0093 \pm 1.9991i,\ -0.0124 \pm 0.3889i,\ -0.0026 \pm 0.1561i,\ -0.0052 \pm 0.0913i\} \tag{24}$$

Figure 10(a) shows that the eigenvalues closest to the $\Im(z) = 0$ axis are most sensitive to perturbation, again these are associated with the motion of the balls. This is confirmed in Fig. 10(b) where a zoom of these eigenvalues shows that the rightmost eigenvalue $\lambda_R = -0.0026 \pm 0.1561i$, is most sensitive to perturbation.

Figure 10(c) shows the rate of decay of the matrix exponential $\|e^{\mathcal{A}t}\|$. An initial growth in the transient is clearly seen which then decays only to grow again. This behaviour repeats until $t \approx 1000$ where we observe an oscillatory decay to stability. As predicted, this final decay follows the curve $f_4(t) = Ce^{\Re(\lambda_R)t}$ where $C > 0$.

Finally, Fig. 10(d) shows the transient behaviour of the full nonlinear system (1) and (2) where we start from an initial condition given by the balanced steady state plus a small perturbation applied to the initial angular position of the balls, that is,

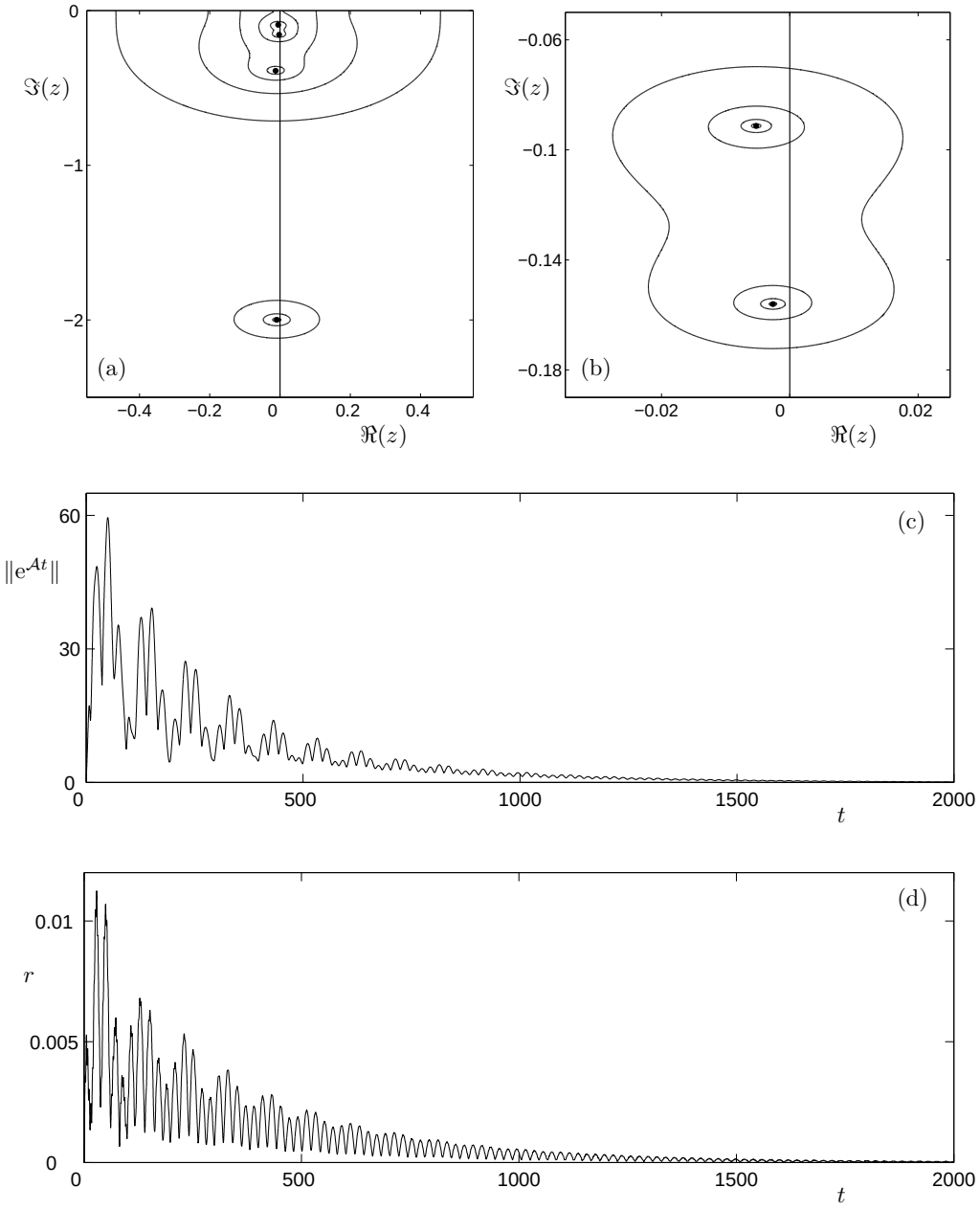


Fig. 10. Pseudospectra and transient behaviour of a balanced steady state solution. Panel (a) shows the $\epsilon$-pseudospectra of the linear eigenvalue problem $\Lambda_\epsilon(\mathcal{A})$. From outermost to innermost, the contours correspond to pseudospectra with $\epsilon = 10^{-1}$, $10^{-1.5}$, $10^{-2}$, $10^{-2.5}$, and $10^{-3}$. Panel (b) shows the $\epsilon$-pseudospectra of the eigenvalues most sensitive to perturbation. From outermost to innermost, the contours correspond to pseudospectra with $\epsilon = 10^{-3}$, $10^{-3.5}$, $10^{-4}$, and $10^{-4.5}$. Panel (c) shows the transient behaviour of the matrix exponential of the linearised system $\|e^{\mathcal{A}t}\|$. Panel (d) shows the transient behaviour of the full nonlinear system where the steady state angular position of the balls was perturbed by $\pi/128$. In all cases, parameters were set to $\Omega = 1.04$, $\zeta = 0.01$, $\beta = 0.01$, $\delta = 0.01$, $\mu = 0.05$.

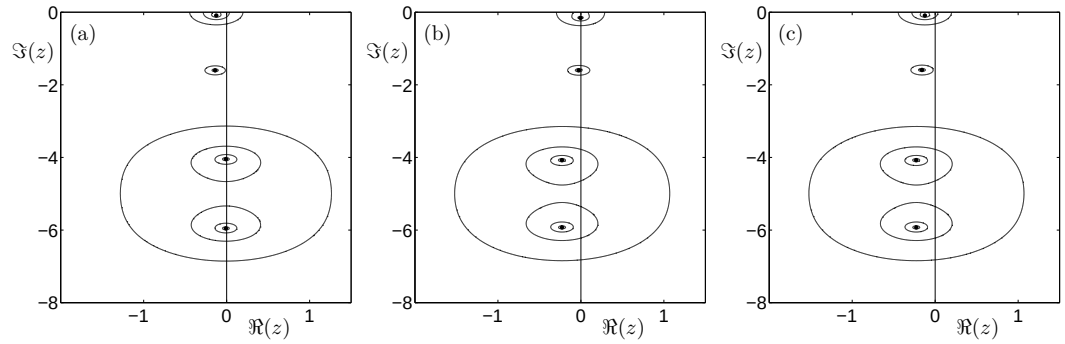


Fig. 11. Pseudospectra of the linear eigenvalue problem $\Lambda_\epsilon(\mathcal{A})$ of a balanced steady state solution. From outermost to innermost, the contours correspond to pseudospectra with $\epsilon = 10^{-1}$, $10^{-1.5}$, $10^{-2}$, and $10^{-2.5}$. Panel (a) shows the pseudospectra for increased damping of the balls $\beta = 0.25$, panel (b) shows the pseudospectra for increased damping of the rotor $\zeta = 0.25$, and panel (c) shows the pseudospectra for both increased damping to the balls and to the rotor $\beta = \zeta = 0.25$. In all cases, other fixed parameters were set to $\Omega = 5$, $\delta = 0.01$, $\mu = 0.05$.

$$\phi_1(0) = -\phi_2(0) = \arccos(-\delta/(2\mu)) + \pi/128 = 1.6955. \tag{25}$$

Once again, the transient is shown to follow the path predicted by the decay of the matrix exponential of the linearised system.

Furthermore, simulations show that this steady state has a small basin of attraction when varying the initial angular position of the balls in this way [7]. In fact, for $\Omega = 1.04$ investigations show that this steady state is only attracting for $\phi_1(0) \in [1.635, 1.720]$, $\phi_2(0) = -\phi_1(0)$. For all other values of $\phi_1(0) \in [0, \pi]$ the attracting state is a stable, coexisting quasiperiodic modulation. Note that a transient growth is always seen regardless of the nature of the attracting state.

## 6 The effect of damping on the pseudospectra and transient response

One would expect that increased damping of the ADB would lead to shorter transients. However, we now show that variations in the external damping ratio of the rotor $\zeta$ and of the internal damping of the balls in the ADB $\beta$ can affect which eigenvalues are most sensitive to perturbation, and hence, not just the length, but also the nature of the transient response of the ADB.

Figure 11 shows the pseudospectra for differing values of these damping coefficients; these pseudospectra were computed using `EIG-TOOL`, and should be compared to Fig. 3(a). In each panel, from outermost to innermost, the con-

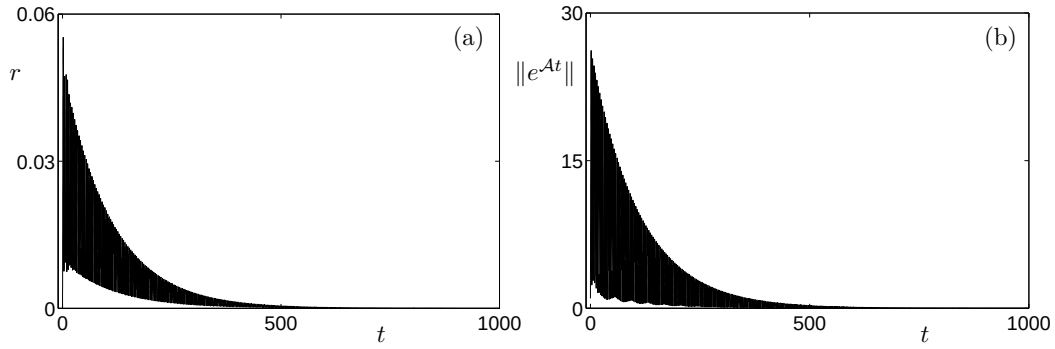


Fig. 12. Transient response when the damping of the balls $\beta$ is increased. Panel (a) shows the behaviour of the full nonlinear system with initial condition $x = y = \dot{x} = \dot{y} = \dot{\phi}_1 = \dot{\phi}_2 = 0$, $\phi_1 = -\pi/2$, and $\phi_2 = \pi/2$, and panel (b) shows the matrix exponential $\|e^{\mathcal{A}t}\|$ of the linearised system. Parameters were set to $\Omega = 5$, $\zeta = 0.01$, $\beta = 0.25$, $\delta = 0.01$, $\mu = 0.05$.

tours correspond to pseudospectra with $\epsilon = 10^{-1}$, $10^{-1.5}$, $10^{-2}$, and $10^{-2.5}$. Fixed parameters were set according to (10). In Fig. 11(a) the damping coefficients were changed to $\beta = 0.25$ and $\zeta = 0.01$. It is clearly seen that the eigenvalues $\lambda_1^{\pm}$ and $\lambda_2^{\pm}$ (rotor modes), furthest from the $\Im(z) = 0$ axis, are most sensitive to perturbation. Specifically, the pseudospectra corresponding to the rightmost eigenvalue $\lambda_2^{\pm} = -9.03 \times 10^{-3} \pm 4.05i$ reaches the right-half plane for $\epsilon = 10^{-3.17}$ and the pseudospectra of the most sensitive eigenvalue $\lambda_1^{\pm} = -9.15 \times 10^{-3} \pm 5.95i$ reaches the right-half plane for $\epsilon = 10^{-3.16}$. For $\beta = 0.01$ and $\zeta = 0.25$, Fig. 11(b) shows that the situation is now reversed, that is, the eigenvalues $\lambda_3^{\pm}$ and $\lambda_4^{\pm}$ (ball modes), closest to the $\Im(z) = 0$ axis, are most sensitive to perturbation. The rightmost eigenvalue $\lambda_4^{\pm} = -4.31 \times 10^{-3} \pm 0.153i$ is the most sensitive to perturbation with the $\epsilon = 10^{-2.89}$ pseudospectra reaching the right-half plane. Finally, Fig. 11(c) shows the effect of increasing both the damping coefficients to $\beta = \zeta = 0.25$. All eigenvalues are seen to move away from the imaginary axis. The rightmost eigenvalue is $\lambda_4^{\pm}$, the one closest to the $\Im(z) = 0$ axis. However, the eigenvalues most sensitive to perturbation are again $\lambda_1^{\pm}$ and $\lambda_2^{\pm}$ (rotor modes), those furthest from the $\Im(z) = 0$ axis. In the latter case, both pseudospectra reach the right-half plane for $\epsilon = 10^{-1.78}$.

We now identify the changes in the pseudospectra shown in Fig. 11 with changes in the transient response of the ADB as the values of the damping coefficients are varied. Figures 12 to 14 show the transient response of the full nonlinear system, where we plot the magnitude of the radial vibration $r$ against time $t$ for initial conditions of $x = y = \dot{x} = \dot{y} = \dot{\phi}_1 = \dot{\phi}_2 = 0$, $\phi_1 = -\pi/2$, and $\phi_2 = \pi/2$, along with the transient response of the matrix exponential of the linearised system $\|e^{\mathcal{A}t}\|$. The parameter values used in Figs. 12 to 14 correspond to those used in Figs. 11(a) to (c), respectively.

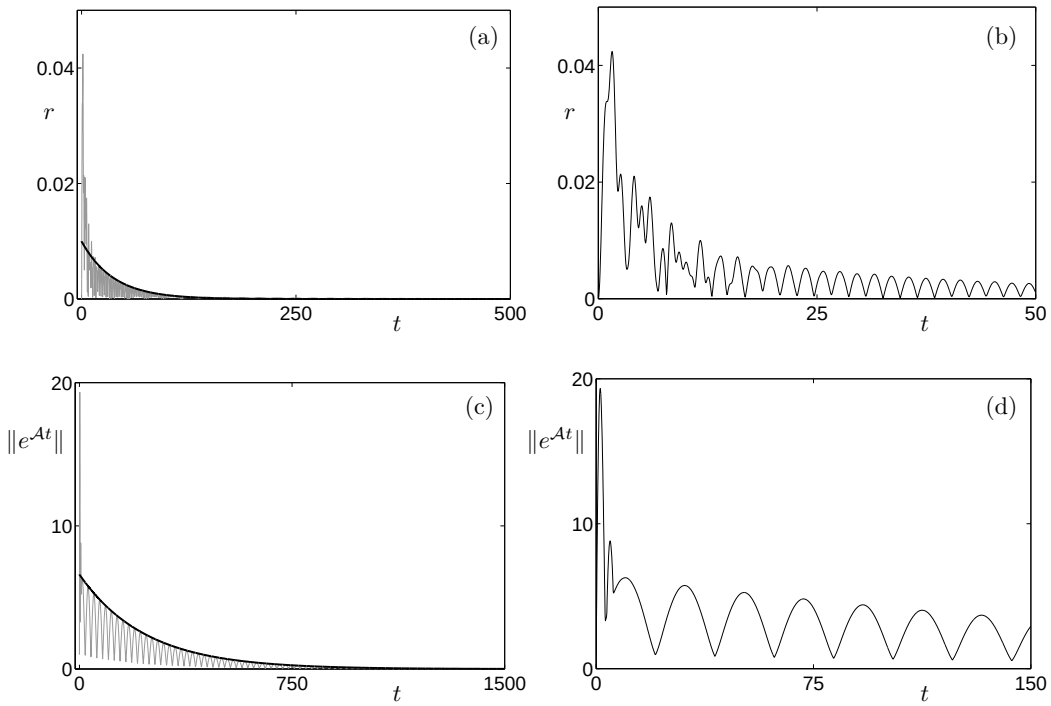


Fig. 13. Transient response when the damping of the rotor $\zeta$ is increased. Panels (a) and (b) show the behaviour of the full nonlinear system with initial condition $x = y = \dot{x} = \dot{y} = \dot{\phi}_1 = \dot{\phi}_2 = 0$, $\phi_1 = -\pi/2$, and $\phi_2 = \pi/2$, and panels (c) and (d) show the matrix exponential $\|\mathrm{e}^{\mathcal{A}t}\|$ of the linearised system. Parameters were set to $\Omega = 5$, $\zeta = 0.25$, $\beta = 0.01$, $\delta = 0.01$, $\mu = 0.05$.

Figure 12(a) shows a typical transient radial vibration for values of damping coefficients $\beta = 0.25$ and $\zeta = 0.01$. The transient is shown to decay exponentially with an underlying, high frequency oscillation; compare this with Fig. 8. Both effects are associated with the eigenvalues furthest from the $\Im(z) = 0$ axis, and rightmost, $\lambda_1^{\pm} = -9.15 \times 10^{-3} \pm 5.95i$ and $\lambda_2^{\pm} = -9.03 \times 10^{-3} \pm 4.05i$, where the real part dictates the exponential decay and the imaginary part the fast oscillation. As was shown in Fig. 11(a), $\lambda_1^{\pm}$ is also the eigenvalue most sensitive to perturbation. This behaviour is mirrored in Fig. 12(b) where we plot the matrix exponential $\|\mathrm{e}^{\mathcal{A}t}\|$ of the linearised system (9).

For values of damping coefficients $\beta = 0.01$ and $\zeta = 0.25$, Fig. 13(a) shows that the transient takes less time. In fact, we see a fast 'collapse' from the initial high amplitude peak to an exponential decay with an underlying oscillation; Fig. 13(b) shows a zoom of this transient. It was shown in Fig. 11(b) that for these values of damping the eigenvalues $\lambda_1^{\pm}$ and $\lambda_2^{\pm}$ (rotor modes), furthest from the $\Im(z) = 0$ axis, are leftmost and least sensitive to perturbation, these do not play a role in the transient behaviour and, hence, the collapse. The exponential decay in Figs. 13(a) and (b) follows the next rightmost eigenvalue $\lambda_3^{\pm} = -2.70 \times 10^{-2} \pm 1.60i$ (indicated by a thick curve) before eventual asymp-

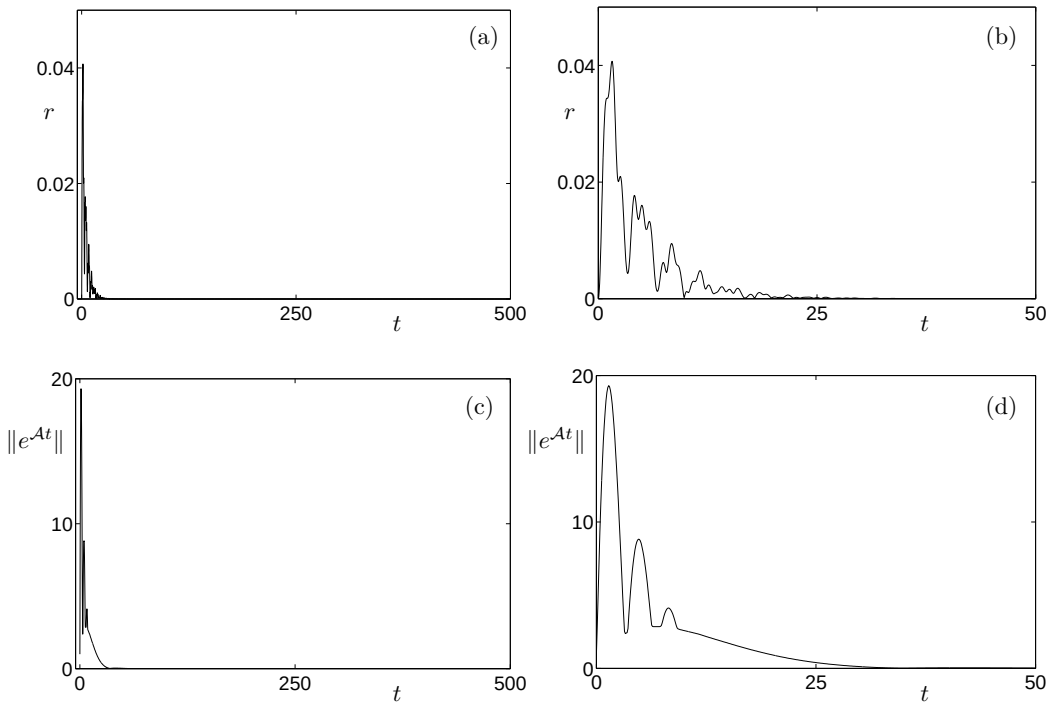


Fig. 14. Transient response when the damping of both the balls $\beta$ and the rotor $\zeta$ is increased. Panels (a) and (b) show the behaviour of the full nonlinear system with initial condition $x = y = \dot{x} = \dot{y} = \dot{\phi}_1 = \dot{\phi}_2 = 0$, $\phi_1 = -\pi/2$, and $\phi_2 = \pi/2$, and panels (c) and (d) show the matrix exponential $\|\mathrm{e}^{\mathcal{A}t}\|$ of the linearised system (c) and (d). Parameters were set to $\Omega = 5$, $\zeta = 0.25$, $\beta = 0.25$, $\delta = 0.01$, $\mu = 0.05$.

totic decay along the rightmost eigenvalue $\lambda_4^{\pm} = -4.31 \times 10^{-3} \pm 0.153i$. This latter eigenvalue $\lambda_4^{\pm}$ is also most sensitive to perturbation; see Fig. 11(b). Figures 13(c) and (d) show the behaviour of the matrix exponential $\|\mathrm{e}^{\mathcal{A}t}\|$. Again, one initially sees a large transient peak before collapse to exponential decay. However, unlike in Figs. 13(a) and (b), this decay always follows the most sensitive eigenvalue $\lambda_4^{\pm}$ (indicated by a thick curve). The different frequencies of oscillation are clearly seen by comparing Figs. 13(b) and (d). However, both $\lambda_3^{\pm}$ and $\lambda_4^{\pm}$ correspond to ball modes and are, therefore, associated with low frequency responses.

Finally we show the effect on the transient response of increasing the values of both damping coefficients to $\beta = \zeta = 0.25$. Figures 14(a) and (b) show that the transient radial vibration is minimal. In fact, after an initial high amplitude peak the transient collapses to the balanced steady state solution. This behaviour mirrors closely the transient response of the matrix exponential $\|\mathrm{e}^{\mathcal{A}t}\|$, shown in Figures 14(c) and (d). It was shown in Fig. 11(c) that for these values of increased damping all eigenvalues are less sensitive to perturbation, compared to those in Figs. 11(a) and (b). The eigenvalue $\lambda_4^{\pm}$ closest to the $\Im(z) = 0$ axis is rightmost and accounts for the eventual asymptotic decay

(this is too small to see in Fig. 14); while the eigenvalues $\lambda_1^{\pm}$ and $\lambda_2^{\pm}$, furthest from the $\Im(z) = 0$ axis, were shown to be most sensitive to perturbation, a large perturbation of $\epsilon = 10^{-1.78}$ was needed to reach the right-half plane and, consequently, the highly oscillatory exponential decay associated with these modes was not observed.

### *6.1 Controlling the size of the initial transient growth*

In Section 5 we noted that a lower bound on the size of the transient growth of the matrix exponential $\|e^{\mathcal{A}t}\|$ is given by $\eta/\epsilon$, where the $\epsilon$-pseudospectra of $\mathcal{A}$ extends a distance $\eta$ into the right-half plane [20]. This result motivates one to consider ways of controlling the size of the transient growth by shifting the pseudospectra to the left or right. In Fig. 11(b) it was shown that increasing the external damping ratio $\zeta$ shifts the eigenvalues $\lambda_1^{\pm}$ and $\lambda_2^{\pm}$ (rotor modes), with largest imaginary part, to the left. Therefore, in Fig. 15(a) we increase the external damping ratio to $\zeta = 1.5$. As predicted, the eigenvalues $\lambda_1^{\pm}$ and $\lambda_2^{\pm}$ and their associated pseudospectra are shifted to the left. The $\epsilon = 10^{-1}$ pseudospectra now extends to $\Re(z) = 0.5984$, thus giving a lower bound on the growth of the matrix exponential of 5.984. Figure 15(c) shows the reduced transient growth of the matrix exponential, while Fig. 15(e) shows a corresponding reduction in the growth of the radial vibration of the full nonlinear system; compare with Fig. 8. However, we warn that increasing the value of external damping ratio to $\zeta > 1.85$ results in the eigenvalue $\lambda_4^{\pm}$ (a ball mode), with smallest imaginary part, becoming unstable [7]. In this case, one observes a dynamic similar to that shown in Fig. 15(e) but with a slow growth in the radial vibration instead of a decay, before an eventual attracting quasiperiodic modulation.

On the other hand, variation of other parameters may cause an increase in the transient growth. Figure 15(b) shows the pseudospectra for $\Omega = 20$. As the rotation speed $\Omega$ is increased, it was identified in Sec. 3 that the ADB becomes increasingly non-normal; see Fig. 2. The eigenvalues $\lambda_1^{\pm}$ and $\lambda_2^{\pm}$ (rotor modes), with large imaginary part, are shown to move down and their associated pseudospectra are shown to extend further into the right-half plane. In fact, the $\epsilon = 10^{-1}$ pseudospectra now extends to $\Re(z) = 6.248$, thus giving a lower bound on the growth of the matrix exponential of 64.248. The initial growth in the matrix exponential is clearly evident in Fig. 15(d). Likewise, the initial growth in the radial vibration of the full nonlinear system increases; see Fig. 15(f). We now discuss what effect a variation of the initial positions of the balls in the ADB, combined with varying damping parameters, has on the dynamics and the transient growth of the system.

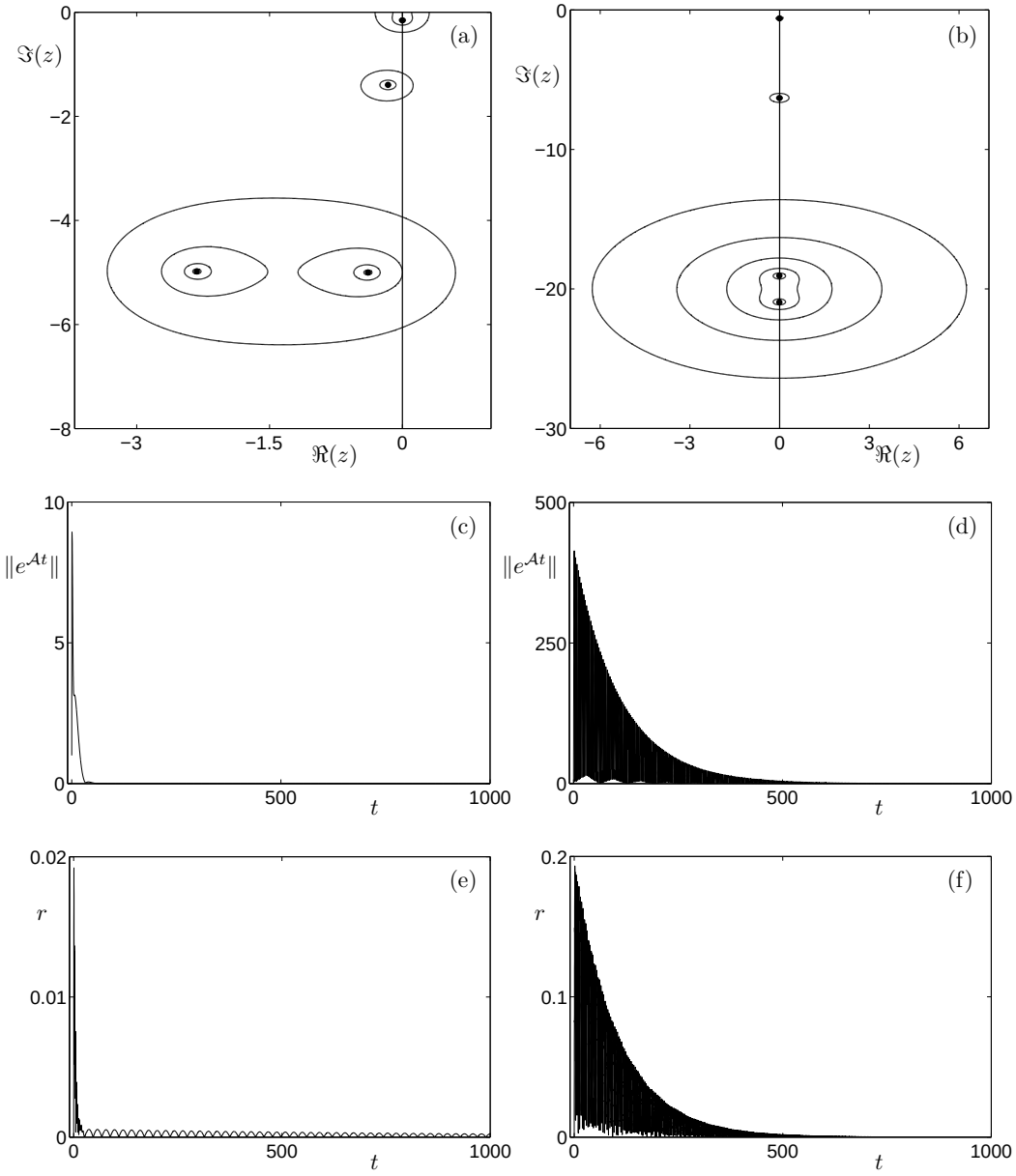


Fig. 15. Pseudospectra and transient behaviour of a balanced steady state solution. Panels (a) and (b) show the $\epsilon$-pseudospectra of the linear eigenvalue problem $\Lambda_\epsilon(\mathcal{A})$. From outermost to innermost, the contours correspond to pseudospectra with $\epsilon = 10^{-1}, 10^{-1.5}, 10^{-2}, 10^{-2.5}$, and $10^{-3}$. Panels (c) and (d) show the transient behaviour of the matrix exponential of the linearised system $\|e^{\mathcal{A}t}\|$. Panels (e) and (f) show the transient behaviour of the full nonlinear system where the steady state angular position of the balls was given as $\phi_1(0) = \pi/2$ and $\phi_2(0) = -\pi/2$. In the first column, parameters were set to $\Omega = 5.0$, $\zeta = 1.5$, $\beta = 0.01$, $\delta = 0.01$, $\mu = 0.05$, and in the second column, parameters were set to $\Omega = 20.0$, $\zeta = 0.01$, $\beta = 0.01$, $\delta = 0.01$, $\mu = 0.05$.

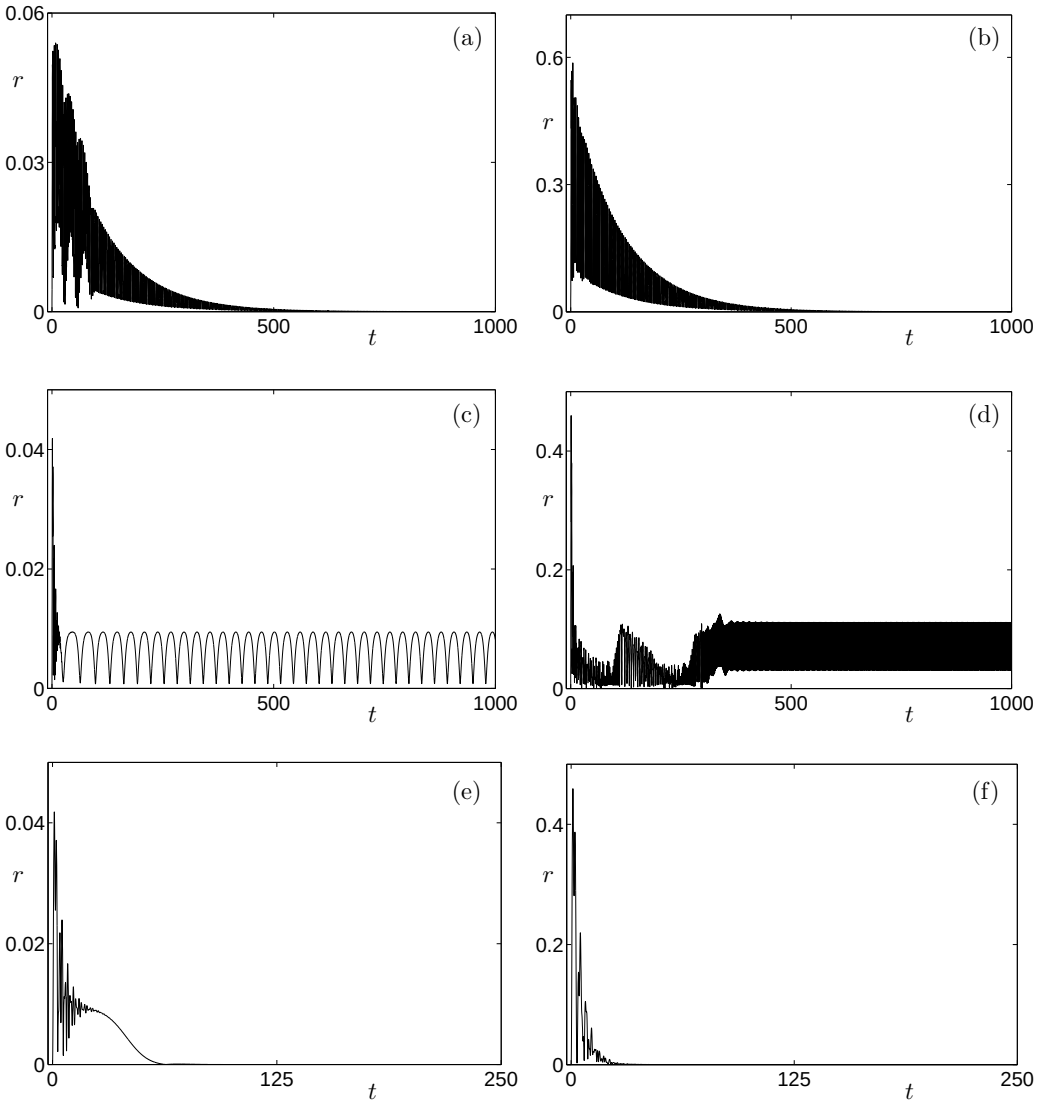


Fig. 16. Transient response of the full nonlinear system when the damping of both the balls $\beta$ and the rotor $\zeta$ is increased. The first column shows the behaviour for initial conditions $x = y = \dot{x} = \dot{y} = \dot{\phi}_1 = \dot{\phi}_2 = 0$, $\phi_1 = 0$, and $\phi_2 = \pi$. The second column shows the behaviour for initial conditions $x = y = \dot{x} = \dot{y} = \dot{\phi}_1 = \dot{\phi}_2 = 0$, $\phi_1 = \pi/128$, and $\phi_2 = -\pi/128$. Damping parameters were set to $\zeta = 0.01$, $\beta = 0.25$ (a) and (b), $\zeta = 0.25$, $\beta = 0.01$ (c) and (d), and $\zeta = 0.25$, $\beta = 0.25$ (e) and (f). In all cases, other parameters were fixed at $\Omega = 5$, $\delta = 0.01$, $\mu = 0.05$.

### *6.2 Variation of initial condition*

Variation of initial conditions has been shown to affect the dynamics of the ADB considerably [7]. Figure 16 shows the effect of varying the initial positions of the balls in the ADB. The first column shows the transient radial vibration of the full nonlinear system for initial ball positions $\phi_1(0) = 0$ and $\phi_2(0) = \pi$, the second column for initial positions $\phi_1(0) = \pi/128$ and $\phi_2(0) = -\pi/128$.

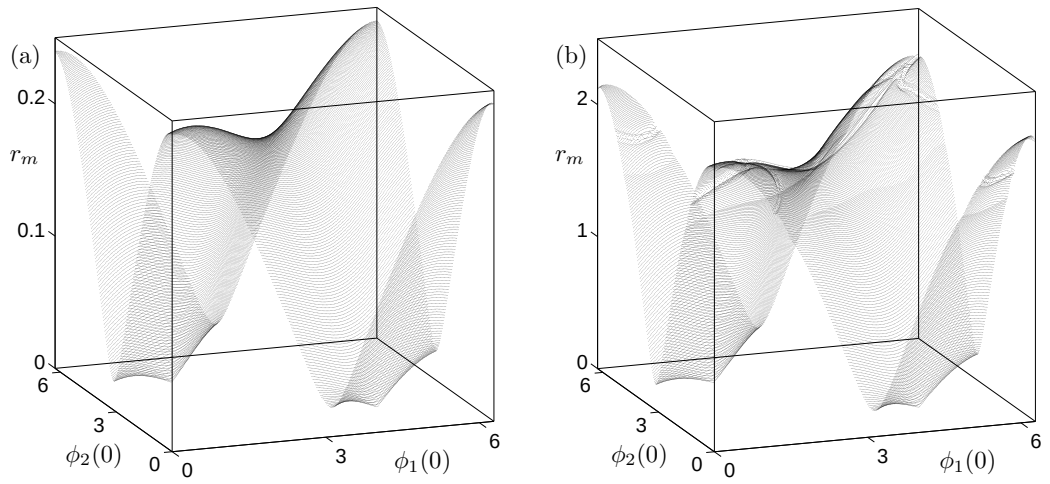


Fig. 17. Maximum amplitude of radial vibration $r_m$ for varying initial positions of the balls $\phi_1(0)$ and $\phi_2(0)$. All other initial conditions were set to zero. In panel (a), parameters were fixed at $\Omega = 5.0$, $\zeta = 1.5$, $\beta = 0.01$, $\delta = 0.01$, and $\mu = 0.05$. In panel (b), parameters were fixed at $\Omega = 20.0$, $\zeta = 0.01$, $\beta = 0.01$, $\delta = 0.01$, and $\mu = 0.05$.

Figures 16(a,b), and (e,f) show the transients for damping coefficients of $\{\zeta = 0.01, \beta = 0.25\}$, and $\zeta = \beta = 0.25$, respectively. These compare well with Figs. 12 and 13 presented in Section 6. However, Figs. 16(c) and (d), for values of damping coefficients $\zeta = 0.25$ and $\beta = 0.01$, show a marked difference to the attracting dynamic shown in Fig. 13. While an initial large amplitude peak in the transient is observed, the attracting dynamics are shown to be two different types of periodic motion. Figure 16(c) shows a periodic motion where both balls continuously rotate, at a constant angular velocity, within the rotating frame. Similarly, Fig. 16(d) shows a periodic motion where one ball comes to rest while the other ball continuously rotates, at a constant angular velocity, within the rotating frame. This is a warning of that the ADB is a highly nonlinear device and an investigation of the attracting dynamics has to include a full nonlinear bifurcation analysis, akin to that of Ref. [7]. Note that the two initial conditions result in a marked difference in the initial value of vibration $r$. In fact, the magnitude of the initial radial vibration for initial positions $\phi_1(0) = 0$ and $\phi_2(0) = \pi$ is ten times smaller than that for $\phi_1(0) = \pi/128$ and $\phi_2(0) = -\pi/128$. We now discuss what effect varying the initial condition has on the size of the transient growth in the full nonlinear system.

Figure 17 shows the maximum radial vibration $r_m$ reached, during the transient period, for varying initial positions of the balls $\phi_1(0)$ and $\phi_2(0)$. The parameters considered correspond to those used in Fig. 15. Specifically, in Fig. 17(a), $\Omega = 5.0$, $\zeta = 1.5$, $\beta = 0.01$, $\delta = 0.01$, and $\mu = 0.05$. While in Fig. 17(b), $\Omega = 20.0$, $\zeta = 0.01$, $\beta = 0.01$, $\delta = 0.01$, and $\mu = 0.05$. In Sec. 6.1 it

was shown that these two parameter sets produced contrasting sizes of transient growths. This is clearly evident in Fig. 17: the size of the maximum radial growth $r_m$ in Fig. 17(a) is approximately ten times larger than that of Fig. 17(b) for similar initial conditions. Moreover, Fig. 17 clearly identifies sets of initial conditions for which the transient growth is minimised or maximised. In general, the initial conditions $\phi_1(0) = \phi_2(0) + 2n\pi$ $(n \in \mathbb{Z})$ correspond to a large growth. Specifically, in Fig. 17(a) this reaches a maximum of $\max(r_m) \approx 0.2400$, while in Fig. 17(b), $\max(r_m) \approx 2.1558$. The initial conditions $\phi_1(0) = \phi_2(0) + (2n+1)\pi$ $(n \in \mathbb{Z})$ correspond to smallest growth. Furthermore, one observes a local minimum at the mid-point of the line $\phi_1(0) = \phi_2(0)$, that is, $\phi_1(0) = \phi_2(0) = \pi$. Moreover, a global minimum in Figs. 17(a) and (b) can be seen to occur when the balls are launched close to the balanced steady state position, $\phi_1 = 1.67096$, $\phi_2 = -1.67096$; trivially, if the balls were launched on the balanced state the growth would be zero.

Finally, Fig. 18 shows the basins of attraction of the balanced steady state for varying initial positions of the balls $\phi_1(0)$ and $\phi_2(0)$. Internal damping was fixed at $\beta = 0.01$, while external damping ratio $\zeta$ was varied from panel to panel. The shaded regions correspond to initial conditions from which the balanced state is attracting, the light regions to initial conditions from which periodic or more complex dynamics are observed. Note that all plots are symmetric about the line $\phi_1(0) = \phi_2(0)$. Figure 18(a) shows that, for $\zeta = 0.01$, the basin of attraction of the balanced state is accessible from most initial ball positions. Exceptions being when the balls are launched from the same position, $\phi_1(0) = \phi_2(0)$, or from a small number of positions about this line. As the external damping ratio $\zeta$ is increased, Fig. 18(b) for $\zeta = 0.1$ shows that the basin of attraction decreases. One observes regions with complex boundaries about the line $\phi_1(0) = \phi_2(0)$ and also when the balls are launched close to the imbalance $\phi_{1,2}(0) = 0$, $\phi_{2,1}(0) = \phi_{1,2}(0) + 2\pi$. Figure 18(c) shows that for $\zeta = 0.2$ these regions, outside the basin of attraction, become broader and their edges become smoother; correspondingly, the shaded region defining the basin of attraction is seen to decrease in size. Finally, Fig. 18(d) for $\zeta = 0.25$ shows a much smaller basin of attraction of the balanced state. Note that the balanced state (3) is, of course, contained within this 'tear-drop' shaped basin of attraction (as it is within each shaded region of Fig. 18). Furthermore, Fig. 18(d) indicates why we observed no convergence to the balanced state in Figs. 16(c) and (d), both the initial positions $(\phi_1(0), \phi_2(0)) = (0, \pi)$ and $(\phi_1, \phi_2(0)) = (\pi/128, -\pi/128)$ are clearly seen to lie outside the basin of attraction of the balanced state. Moreover, we note that an investigation of a variation of the internal damping $\beta$ was shown to cause little change in the size or shape of the basin of attraction of the balanced state. In fact, for $\beta > 0.05$, the only initial conditions which did not converge to the balanced state were the ones along the line $\phi_1(0) = \phi_2(0)$, that is, when the balls where launched from the same position.

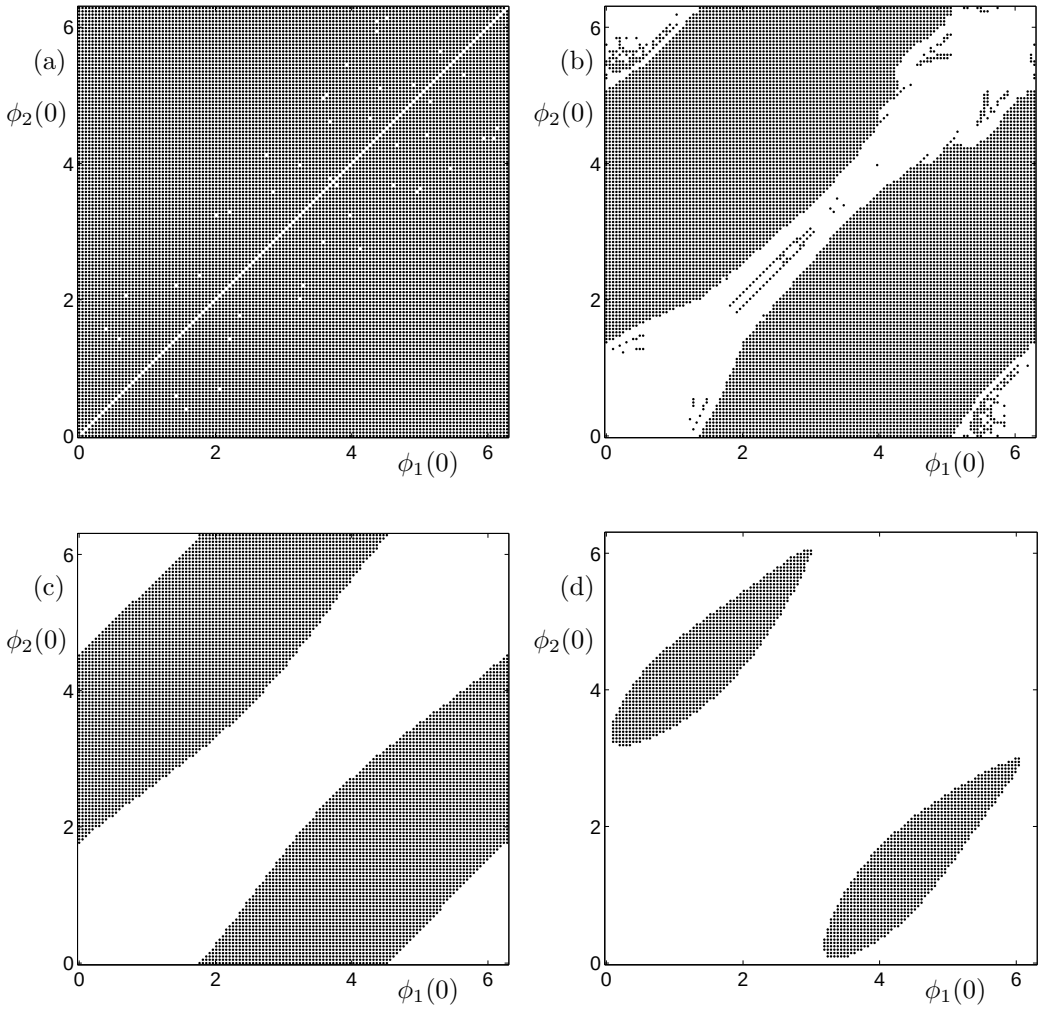


Fig. 18. Basins of attraction of the balanced state for varying initial positions of the balls $\phi_1(0)$ and $\phi_2(0)$. All other initial conditions were set to zero. Parameters were fixed at $\Omega = 5$, $\beta = 0.01$, $\delta = 0.01$, $\mu = 0.05$. From (a) to (d), the external damping ratio $\zeta$ was given values 0.01, 0.1, 0.2 and 0.25. Shaded regions correspond to initial positions from which the balanced state is attracting.

## 7 Conclusion

In many applications involving rotating machinery it is important to know which frequencies may be excited after perturbation. In particular, the degree and nature of the transient response to perturbation can be highly unpredictable. This is evident in the non-normality of the damping and stiffness matrices describing such systems. To this end, we have investigated the transient response and sensitivity to perturbation of an eccentric rotor fitted with an ADB. Using advanced numerical techniques, pseudospectra of both first-order and second-order systems describing the ADB were computed. This allowed us to identify the sensitivity to perturbation of individual eigenvalues, or modes,

in the system. Interestingly, for the second-order model, it was shown that a variation of the weight of the individual matrices of this quadratic description resulted in changes to which eigenvalue was most sensitive to perturbation. This may be an important consequence in modelling a physical device where one may think of structured perturbations to the mass, damping and stiffness matrices as, for example, fouling of turbine blades, or wear in machine tools.

The characteristic large amplitude, fast transients of the full nonlinear system describing the ADB were investigated. The rate of decay of these transients was shown to be directly related to the decay from a transient growth in the matrix exponential describing the evolution of the stable, linearised system. This transient growth phenomena is again a result of the high non-normality of the ADB. Furthermore, for low values of damping, it was shown that the trajectory decayed at a rate according to the most sensitive eigenvalue, not necessarily the right-most. Note that the nature of the transient dynamic, obtained by numerical integration, agreed more closely with that predicted by the pseudospectra of the first-order system rather than that predicted by the structured pseudospectra of the second-order system. This is a warning that while it may be intuitive to study structured perturbations, this approach may not always give the most accurate results.

In a practical design, the amount of internal damping applied to the balls in the ADB, or the external damping of the entire rotor system is accessible and can be easily varied. This led to an investigation into how the transient response depended on these parameters, and whether, or not, the damping could be be varied in order to minimise the length of the transient. Indeed, our results showed that by varying the damping parameters, the eigenvalues most sensitive to perturbation changed and thus the transient behaviour varied. Specifically, for all values of damping a large transient growth was observed. This growth decayed in various ways. In the case of increased internal damping the transient followed a highly oscillatory exponential decay. For an increased external damping ratio, the trajectory was shown to suddenly collapse before eventual asymptotic decay. For both increased internal and external damping, after the initial transient growth, the trajectory also collapsed to the balanced steady state. This motivated the result that the length of the transient could be minimised by simply increasing the size of the external damping ratio. However, we were warned that increasing the external damping ratio too far could lead to the loss of an attracting balanced state.

Finally, we were reminded of the nonlinearities present in the full ADB model. It was shown that for different initial conditions, after an initial transient growth, the system trajectory may be attracted to unwanted periodic oscillations. This was shown to be due to the size of the basin of attraction of the balanced steady state shrinking as the external damping ratio was increased. Another warning that one must balance the want of decreasing the length of

transient response by increasing the external damping ratio with the threat of unwanted instabilities.

## Acknowledgements

This work was funded by the EPSRC grant GR/535684/01. The authors wish to thank T. Wagenknecht, J. Agarwal, P. Lancaster and P. Psarrakos for providing the code allowing computation of structured pseudospectra. Professor Friswell gratefully acknowledges the support of the Royal Society through a Royal Society-Wolfson Research Merit Award.

## References

[1] J. Adolfsson. *Passive Control of Mechanical Systems: Bipedal Walking and Autobalancing*. PhD thesis, Royal Institute of Technology, Stockholm, 2001.

[2] P. Bövik and C. Högfors. Autobalancing of rotors. *Journal of Sound and Vibration*, 111(3):429–440, 1986.

[3] J. Chung and D. S. Ro. Dynamic analysis of an automatic dynamic balancer for rotating mechanisms. *Journal of Sound and Vibration*, 228(5):1035–1056, 1999.

[4] E. Doedel, A. Champneys, T. Fairgrieve, Yu. Kuznetsov, B. Sandstede, and X. Wang. AUTO 97: Continuation and bifurcation software for ordinary differential equations, 1997. `http://indy.cs.concordia.ca/auto/main.html`.

[5] M. Embree and L. N. Trefethen. *Pseudospectra Gateway*. `http://www.comlab.ox.ac.uk/pseudospectra`.

[6] T. Gebhardt and S. Grossmann. Chaos transition despite linear stability. *Phys. Rev. E*, 50(5):3705–3711, 1994.

[7] K. Green, A. R. Champneys, and N. J. Lieven. Bifurcation analysis of an automatic dynamic balancing mechanism for eccentric rotors. Technical report, University of Bristol, 2004. `http://www.enm.bris.ac.uk/anm/preprints/2004r19.html`.

[8] D. J. Higham and L. N. Trefethen. Stiffness of ODEs. *BIT*, 33:285–303, 1992.

[9] D. Hinrichsen and A. J. Pritchard. On the transient behaviour of stable linear sytems. In *Proceedings of the Fourteenth International Symposium of Mathematical Theory of Networks and Systems*, 2000. http://www.univ-perp.fr/mtns2000/.

[10] W.-Y. Huang, C.-P. Chao, J.-R. Kang, and C.-K. Sung. The application of ball-type balancers for radial vibration reduction of high-speed optic drives. *Journal of Sound and Vibration*, 250(3):415–430, 2002.

[11] W. Kim and J. Chung. Performance of automatic ball balancers on optical disc drives. *Proc Instn Mech Engrs Part C: J Mechanical Engineering Science*, 216(1071–1080), 2002.

[12] P. Lancaster. *Lambda-matrices and vibrating systems*, volume 94 of *Pure and Applied Mathematics*. Pergamon Press, 1966.

[13] P. Lancaster and P. Psarrakos. On the pseudospectra of matrix polynomials. Technical Report 445, University of Manchester, 2004. `http://www.maths.man.ac.uk/~nareports/narep445.pdf`.

[14] J. Lee and W. K. Van Moorhem. Analytical and experimental analysis of a self-compensating dynamic balancer in a rotating mechanism. *ASME Journal of Dynamic Systems, Measurement and Control*, 118:468–475, 1996.

[15] T. Majewski. Synchronous vibration eliminator for an object having one degree of freedom. *Journal of Sound and Vibration*, 112(3):401–413, 1987.

[16] R. Rajalingham and S. Rakheja. Whirl suppression in hand-held power tool rotors using guided rolling balancers. *Journal of Sound and Vibration*, 217(3):453–466, 1998.

[17] R. S. Sharp. An analysis of a self-balancing system for rigid rotors. *J. Mech. Engng. Sci.*, 17(4):186–189, 1975.

[18] E. Thearle. A new type of dynamic-balancing machine. *Transactions of ASME*, 54(APM-54-12):131–141, 1932.

[19] F. Tisseur and N. J. Higham. Structured pseudospectra for polynomial eiegnvalue problems, with applications. *SIAM J. Matrix Anal. Appl.*, 23(1):187–208, 2001.

[20] L. N. Trefethen. Computation of Pseudospectra. *Acta Numerica*, pages 1–46, 1999.

[21] L. N. Trefethen, A. E. Trefethen, S. C. Reddy, and T. A. Driscoll. Hydrodynamic stability without eigenvalues. *Science*, 261(5121):578–584, 1993.

[22] T. Wagenknecht and J. Agarwal. Structured pseudospectra in structural engineering. Technical Report, Univeristy of Bristol, 2004. `http://seis.bris.ac.uk/~enxtw/strucps.pdf`

[23] T. G. Wright. *EIG-TOOL*. Oxford University, 2002. `http://www.comlab.ox.ac.uk/pseudospectra/eigtool/`.